ANALYTICAL SOLUTIONS FOR EVOLUTION AND RUNUP OF LONG WAVES OVER A SLOPING BEACH

A THESIS SUBMITTED TO
THE GRADUATE SCHOOL OF NATURAL AND APPLIED SCIENCES
OF
MIDDLE EAST TECHNICAL UNIVERSITY

BY

NİHAL CEYLAN

IN PARTIAL FULFILLMENT OF THE REQUIREMENTS
FOR
THE DEGREE OF MASTER OF SCIENCE
IN
ENGINEERING SCIENCES

SEPTEMBER 2019

Approval of the thesis:

ANALYTICAL SOLUTIONS FOR EVOLUTION AND RUNUP OF LONG WAVES OVER A SLOPING BEACH

submitted by **NİHAL CEYLAN** in partial fulfillment of the requirements for the degree of **Master of Science in Engineering Sciences Department, Middle East Technical University** by,

Prof. Dr. Halil Kalıpçılar
Dean, Graduate School of **Natural and Applied Sciences** _____

Prof. Dr. Murat Dicleli
Head of Department, **Engineering Sciences** _____

Assoc. Prof. Dr. Utku Kânoğlu
Supervisor, **Aerospace Engineering, METU** _____

Assist. Prof. Dr. Baran Aydın
Co-supervisor, **Civil Engineering, ATU** _____

Examining Committee Members:

Prof. Dr. Ahmet Cevdet Yalçıner
Civil Engineering, METU _____

Assoc. Prof. Dr. Utku Kânoğlu
Aerospace Engineering, METU _____

Assist. Prof. Dr. Baran Aydın
Civil Engineering, ATU _____

Prof. Dr. Zülfü Aşık
Engineering Science, METU _____

Prof. Dr. Hakan I. Tarman
Mechanical Engineering, METU _____

Date:

I hereby declare that all information in this document has been obtained and presented in accordance with academic rules and ethical conduct. I also declare that, as required by these rules and conduct, I have fully cited and referenced all material and results that are not original to this work.

Name, Surname: Nihal Ceylan

Signature :

ABSTRACT

ANALYTICAL SOLUTIONS FOR EVOLUTION AND RUNUP OF LONG WAVES OVER A SLOPING BEACH

Ceylan, Nihal
M.S., Department of Engineering Sciences
Supervisor: Assoc. Prof. Dr. Utku Kânoğlu
Co-Supervisor: Assist. Prof. Dr. Baran Aydın

September 2019, 49 pages

The initial value problem of the linear evolution and runup of long waves on a plane beach is analyzed analytically. The shallow water-wave equations are solved by integral transform and eigenvalue expansion methodologies. The results from linear solutions are compared with the solution of the nonlinear shallow water-wave equations confirming the runup invariance, i.e. nonlinear and linear theories produce same maximum runup. Then, existing analytical nonlinear solution for shoreline motion is implemented for the waveforms given for near-shore earthquakes producing results exactly compared with existing ones, but with a much simpler algebra.

Keywords: Tsunami, shallow water-wave equations, wave runup/rundown, analytical solution

ÖZ

UZUN DALGALARIN GELİŞİMİ VE SABİT EĞİMLİ KUMSALA TIRMANMASI İÇİN ANALİTİK ÇÖZÜMLER

Ceylan, Nihal
Yüksek Lisans, Mühendislik Bilimleri Bölümü
Tez Yöneticisi: Doç. Dr. Utku Kânoğlu
Ortak Tez Yöneticisi: Dr. Öğr. Üyesi Baran Aydın

Eylül 2019 , 49 sayfa

Sabit eğimli kumsala tırmanan uzun dalgaların tırmanması ve doğrusal gelişiminin başlangıç değer problemi analitik olarak ele alınmıştır. Sığ su-dalga denklemleri, integral dönüşümü ve özdeğer açılımı yöntemleri ile çözülmüştür. Doğrusal çözümlerden elde edilen sonuçlar, tırmanmanın değişmezliğini doğrulamak için doğrusal olmayan sığ su-dalga denklemlerinin çözümünden elde edilen sonuçlarla karşılaştırılmıştır. Bu karşılaştırmada, doğrusal ve doğrusal olmayan teorilerin aynı maksimum tırmanma değerlerine sahip olduğu görülmektedir. Daha sonra, kıyı şeridi hareketini inceleyen mevcut doğrusal olmayan analitik çözüm yöntemi, kıyıya yakın depremlerle oluşan dalga formlarına uygulanmıştır. Elde edilen sonuçlar, mevcut çözüm yönteminden elde edilen sonuçlarla karşılaştırıldığında sunulan yöntemin aynı sonuçları mevcut yönteme kıyasla daha basit cebir kullanarak verdiği görülmektedir.

Anahtar Kelimeler: Tsunami, sığ su-dalga denklemleri, dalga tırmanması, analitik çözüm

To my beloved family

ACKNOWLEDGMENTS

First and foremost, I would like to express my gratitude to my advisor Assoc. Prof. Dr. Utku Kânoğlu, who has supported me since the beginning of my studies with his patience and guidance. He always encouraged me in all the time of research and writing of this thesis. I would like to appreciate to my co-supervisor Assist. Prof. Dr. Baran Aydın for his endless and very valuable supports, academic supervision and recommendations about my research, and for giving me strength during my studies.

My sincere gratitude also goes to Prof. Dr. Ahmet Cevdet Yalçıner for his invaluable support, encouragement and great sympathy throughout both my whole undergraduate and graduate life. Besides my supervisors and Prof. Dr. Ahmet Cevdet Yalçıner, I would like to thank the rest of my thesis committee: Prof. Dr. Zülfü Aşık and Prof. Dr. Hakan I. Tarman for their valuable time to participate in my thesis defense and their valuable comments and suggestions.

I would like to thank my parents, Nail and Nilgün, and my cousin, Ceren, and my whole relatives, who have supported and loved me in every moment of my life, and believe in me, I would never survive without their love. I also would like to thank my budgerigar Cacık for his company and giving me a reason to smile.

Thanks to all of my friends, specially Semih Aktaş, Selis Çelik, Berna Başdoğan Bozkır and Mehmet Soylu for their help, kindness and motivation. I also thank METU Subaqua Society for providing not only crossing my road with very valuable people but also supporting me to find myself under the sea.

Finally, I want to thank to the Scientific and Technological Research Council of Turkey (TÜBİTAK). This work is financially supported by TÜBİTAK-BİDEB National scholarship Programme for MSc Students (2210-A).

TABLE OF CONTENTS

LIST OF TABLES

TABLES

LIST OF FIGURES

FIGURES

LIST OF ABBREVIATIONS

CG	Carrier–Greenspan
LDN	Leading Depression N-wave
LEN	Leading Elevation N-wave
NGDC	National Geophysical Data Center
NOAA NCEI	United States National Oceanic and Atmospheric Administration's National Centers for Environmental Information
WDS	World Data Service

CHAPTER 1

INTRODUCTION

Shallow water-waves, which are also called long waves, are ocean waves with wavelength (L) much larger compared to the water depth (d) over which they are propagating, i.e., $L >> d$. Tsunamis are long waves, and they are generated by an impulsive movement of the ocean floor such as an underwater earthquake, volcanic eruption and submarine or subaerial landslides. When ocean floor is disturbed suddenly, it is commonly accepted that this displacement is instantaneously transferred to ocean surface, hence tsunami occurs. In an open sea, tsunami may not be noticed because of its much smaller amplitude compared to its wavelength. As it reaches shallower water; its wavelength becomes smaller and its speed is reduced, according to shallow water-wave speed, $c = \sqrt{gd}$, where g is the gravitational acceleration.

Tsunamis are high-impact and long-duration disasters, often with multiple waves attacking target coastlines, challenging rescue efforts (Kânoğlu et al., 2015). Tsunami as a Japanese word is the combination of 'tsu' and 'nami', meaning 'harbor wave' in English. It became known after the damage of the 1896 Great Meiji Tsunami. It was realized by fishermen after they returned to the port and found the village surrounding the harbor devastated by an enormous wave although they had not been aware of anything unusual while fishing in the open sea. There are authentic records related to these type of waves dated back to the 9th Century AD in Japan. However, the first historical report of coastal inundation by tsunamis refers to the eruption of the Thera volcano in the eastern Mediterranean, which is believed to occur around 1620 BC (Kânoğlu and Synolakis, 2015).

According to the United States National Oceanic and Atmospheric Administration's

National Centers for Environmental Information (NOAA NCEI[1]), tsunamis have cost over 400,000 people's lives since 1850 (NOAA, 2018). Also, according to historical tsunami records, tsunamis mostly occur in oceans –specifically the Pacific Ocean with a share of 70%– and open seas (International Tsunami Information Center, 2018), Figure 1.1.

The deadliest tsunami in recorded history is the 26 December 2004 Indian Ocean tsunami. It is also one of the largest earthquakes in the recorded history (Rabinovich and Thomson, 2007), with the rupture length of almost $1600\ km$ long. This disaster claimed the loss of more than 220,000 lives and devastation throughout the Bay of Bengal (Bilek et al., 2007). According to the post-disaster investigations the wave height reached over $30\ \ m$ in some areas and affected at least 16 nations directly across the Indian Ocean (Synolakis and Kong, 2006; Kânoğlu et al., 2019). The economic impact of this tsunami is about $10 billion and the world's response was an unprecedented, $13.5 billion in international aid (Bernard and Robinson, 2009).

Again, the primary assumption of the shallow water theory is that the horizontal scales (e.g., wavelength, L) are much larger than the vertical scales (e.g., water depth, d, or wave height, H). Therefore, vertical momentum exchange is negligible and the vertical velocity component is much smaller than the horizontal components. The vertical momentum equation is then reduced to a hydrostatic pressure equation and, after averaging the continuity and momentum equations over the depth, the resulting equations employ only two spatial variables, in addition to the temporal variable.

The study of tsunami science has initiated from laboratory experiments with a focus on wave runup. The initial model for tsunamis was a solitary wave, which is a single wave preserving its shape when propagating over a constant depth. Hall and Watts (1953) studied, the 1+1 canonical problem –a one-dimensional single long wave, generated over a constant-depth basin and then climbing up on a uniformly sloping beach.

[1] It is formerly known as National Geophysical Data Center (NGDC).

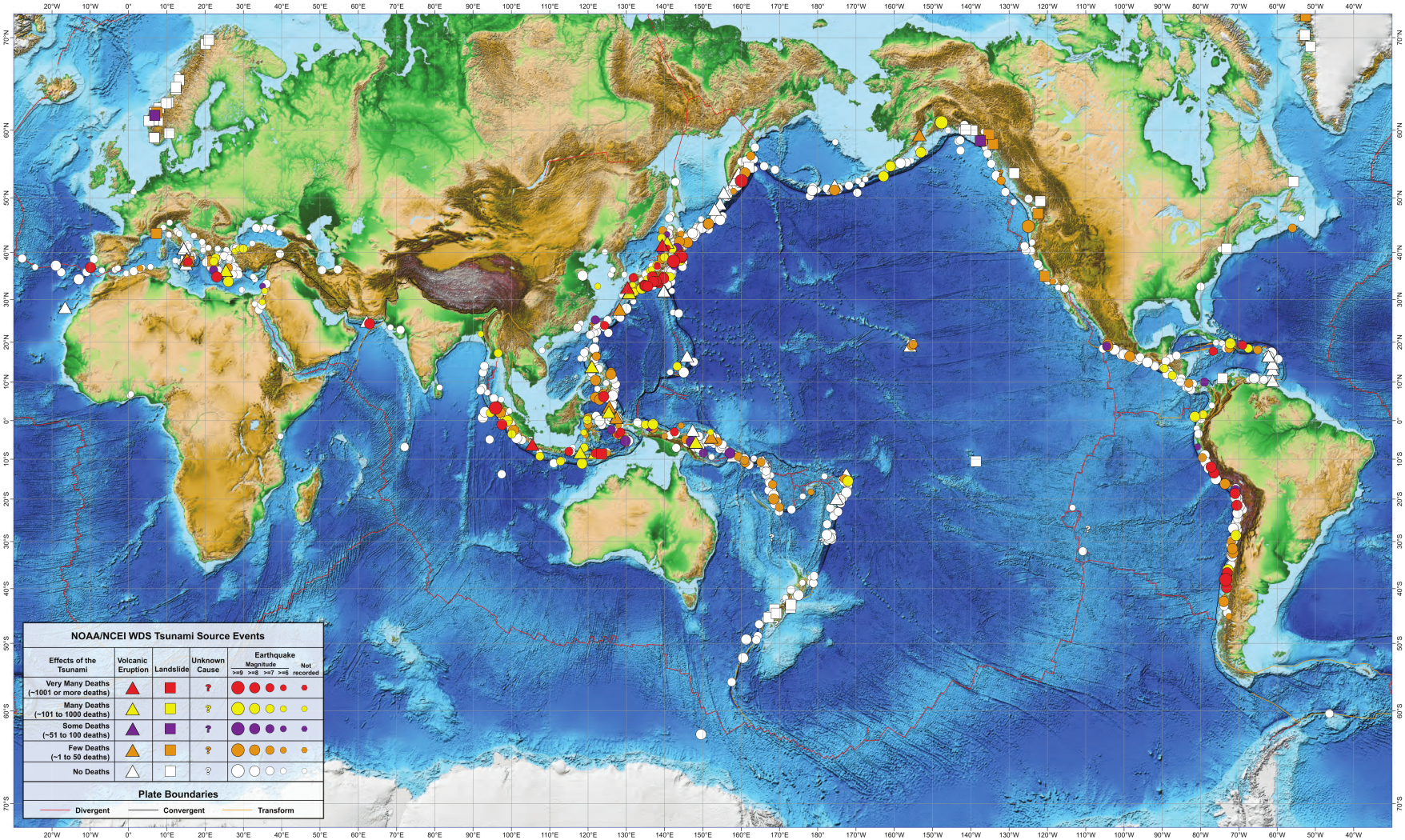

Figure 1.1: Tsunami sources from 1610 BC to AD 2017 (International Tsunami Information Center, 2019).

Carrier and Greenspan (1958) contributed significantly to the initial value problem solutions of the 1+1 dimensional nonlinear shallow water-wave equations introducing a nonlinear transformation, which is now known as Carrier–Greenspan (CG) transformation. They transformed the nonlinear shallow water-wave equations into a single second-order linear Bessel-type equation by substituting the physical variables (x and t) with auxiliary variables (σ and λ). After their transformation the shoreline, which moves up and down over a beach, becomes a fixed point ($\sigma = 0$) in the transform space. Unfortunately, their study remained unused for a long time due to mainly difficulty to define an initial wave in the transform space given in the physical space. Afterwards, Keller and Keller (1964) derived a Bessel-type equation by using linear shallow water-wave equations. They acquired an amplification factor dependent on initial wave height (H) by considering periodic waves over a constant depth at the toe of the beach.

In the 1980s, the results obtained from analytical methods were coupled with experimental results. In particular, Synolakis (1987) made contribution to evolution and runup of solitary waves both propagating over a constant depth and then evolving over a sloping beach as an initial value problem solution of the nonlinear shallow water-wave equation including reflection. He linearized the CG transformation to generalize the initial offshore conditions neglecting nonlinear effects far from the shore. He also utilized Keller and Keller (1964) formulae to define the boundary condition at the toe of the beach. Synolakis (1987) also verified his analytical solutions with experimental results and derived a formula which is known as the runup law to predict the maximum runup for nonbreaking waves.

Tadepalli and Synolakis (1994) offered *N*-wave shape as a leading waves of a tsunami. They defined two different waveforms named as leading elevation *N*-waves (LEN) and leading depression *N*-waves (LDN) depending on whether crest or trough is observed first, respectively. They showed that *N*-waves are more suitable to represent leading wave of a tsunami compared with solitary waves, a claim which was not accepted at first, but confirmed after studies on events such as the 1992 Nicaraguan tsunami.

Carrier et al. (2003) used hodograph transformation over a uniformly sloping beach

to solve 1+1 nonlinear initial value problem with Green's function representation to have more accurate runup computations. Their solution contains integrals with singularities. Kânoğlu (2004) overcame these difficulty using original solution of Carrier and Greenspan (1958) and with linearization of the transformation in space at $t = 0$, and validated the results with Carrier et al. (2003). Tinti and Tonini (2005) used CG transformation to calculate runup of waves produced by near-shore earthquakes. They used different earthquake parameters to create various initial waveforms and then discuss their effect on wave height amplification at the coast. Kânoğlu (2004)'s study is extended for nonzero initial velocity conditions by Kânoğlu and Synolakis (2006). More recently, Aydın (2011) solved the nonlinear shallow water-wave equations as an initial-boundary value problem. He combined the CG transformation with eigenvalue expansion, and obtained propagation and runup of different initial waveforms having zero and nonzero initial velocities. His solution does not only compare well with existing literature, but it is also more general and computationally efficient.

In this study, first, the linear shallow water-wave equations are solved by using an approach which is similar to the methodology of Carrier and Greenspan (1958). In this method, integral transformation is used for reformulation of the free surface problem. Then, solution method employing eigenfunction expansion, similar to Aydın (2011), is presented. Then, both solution methodologies are implemented to calculate the shoreline wave heights and shoreline velocites for the Gaussian waveforms with zero and nonzero initial velocity. Then, new formulations for shoreline quantities, shoreline wave height and velocity, are developed for near-shore earthquakes following Kânoğlu (2004), as an alternative to Tinti and Tonini (2005)'s methodology based on nonlinear shallow water-wave equations.

CHAPTER 2

ANALYTICAL SOLUTIONS OF THE LINEAR SHALLOW WATER-WAVE EQUATIONS

In this chapter, the linear shallow water-wave equations over a sloping beach are solved similar to the solutions of the nonlinear shallow water-wave equations given by Carrier and Greenspan (1958), and Aydın and Kânoğlu (2017). In the former solution methodology, integral transformation is used whereas the latter employs eigenvalue expansion method. The results are compared with the nonlinear solution of Kânoğlu (2004) for the free-surface elevation and shoreline quantities, i.e. shoreline wave height and velocity, for different initial wave profiles.

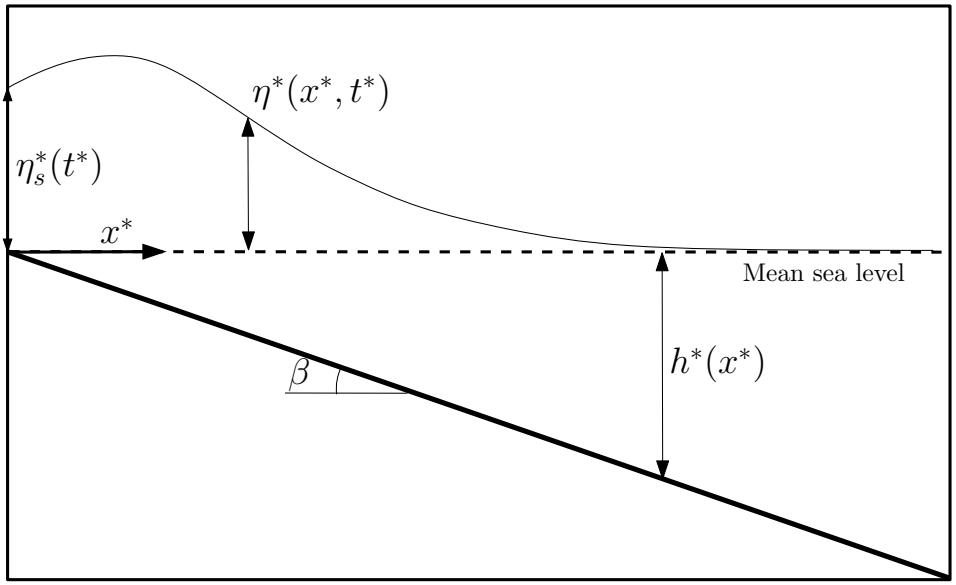

Figure 2.1: The definition sketch (not to scale).

2.1 Governing Equations

In dimensional form, the linear shallow water-wave equations are

$$u^*_{t^*} + g^* \eta^*_{x^*} = 0, \tag{2.1a}$$

$$\eta^*_{t^*} + \left(h^* u^*\right)_{x^*} = 0, \tag{2.1b}$$

where $u^* = u^*(x^*, t^*)$ represents the depth-averaged velocity, $\eta^* = \eta^*(x^*, t^*)$ represents the free-surface disturbance with respect to mean sea level, and $h^*(x) = x^* \tan\beta$ is the local water depth ($x^* \geq 0$, $t^* \geq 0$). β is the angle the beach makes with horizontal, and g^* is the gravitational acceleration (Figure 2.1).

The dimensionless quantities are defined as

$$x = \frac{x^*}{l_0^*}, \quad t = \frac{t^*}{\sqrt{l_0^*/g^* \, \tan\beta}}, \quad \eta, \, h = \frac{\eta^*, \, h^*}{l_0^* \, \tan\beta}, \quad u = \frac{u^*}{\sqrt{l_0^* \, g^* \, \tan\beta}}, \tag{2.2}$$

where l_0^* is a characteristic length scale. Then, the dimensional linear shallow water-wave equations (2.1) takes the following form

$$u_t + \eta_x = 0, \tag{2.3a}$$

$$\eta_t + \left(h \, u\right)_x = 0. \tag{2.3b}$$

Substituting equation (2.3a) into the equation (2.3b) and writing $h(x) = x$, the following second-order linear partial differential equation is obtained as

$$\eta_{tt} = \left(x \eta_x\right)_x. \tag{2.4}$$

This equation is subject to initial and boundary conditions, which are specified in the next section.

2.2 New Solution Methodologies

In the following subsections, two new solution methodologies for the linear shallow water-wave equation (2.4) over a sloping beach are introduced.

2.2.1 Integral Transform Formulation

In this subsection, linear shallow water-wave equation (2.4) will be solved in the infinite domain, $0 \leq x$ and $0 \leq t$. Assuming a time-harmonic dependence of the form

$$\eta(x,t) = A(x)\, e^{-iwt}, \tag{2.5}$$

the linear governing equation (2.4) becomes

$$x\, A''(x) + A'(x) + w^2\, A(x) = 0. \tag{2.6}$$

Equation (2.6) is a Bessel-type equation and its general solution is given as

$$A(x) = C_1\, J_0(2w\sqrt{x}) + C_2\, Y_0(2w\sqrt{x}), \tag{2.7}$$

where J_0 and Y_0 are the first and the second kind Bessel functions of order zero, and C_1 and C_2 are arbitrary constants. Bounded solution at the shoreline, i.e. $\eta(x = 0, t) = finite$, requires C_2 to be zero since $Y_0(2w\sqrt{x}) \to -\infty$ when $x \to 0$. Hence, the solution of equation (2.6) will be

$$A(x) = C\, J_0(2w\sqrt{x}). \tag{2.8}$$

Hence, the solution of equation (2.4) is

$$\eta(x,t) = C\, J_0(2w\sqrt{x})\, e^{-iwt}.$$

The governing equation (2.4) will assume the superposition of all such solutions as general solution, since it is a linear differential equation.

At the initial time ($t = 0$) this general solution can be written as

$$\eta_0(x) = \int_0^\infty C(w)\, J_0(2w\sqrt{x})\, dw. \tag{2.9}$$

Here, the Hankel transform of order ν is introduced as

$$F(k) = \int_0^\infty f(r)\, J_\nu(kr)\, r\, dr, \tag{2.10}$$

where J_ν is the Bessel function of order ν with $\nu \geq -1/2$. The inverse Hankel transform of $F(k)$ is then given as

$$f(r) = \int_0^\infty F(k)\, J_\nu(kr)\, k\, dk. \tag{2.11}$$

The initial waveform, equation (2.9), is apparently the Hankel transform of zero order with $w = r$, $f(r) = \frac{C(w)}{w}$, and $k = 2\sqrt{x}$;

$$\eta_0(x) = \int_0^\infty \frac{C(w)}{w}\, J_0(2w\sqrt{x})\, w\, dw. \tag{2.12}$$

Then inverse Hankel transform, according to (2.11), reads

$$\frac{C(w)}{w} = \int_0^\infty \eta_0(x)\, J_0(2w\sqrt{x})\, (2\sqrt{x})\, \frac{dx}{\sqrt{x}}, \tag{2.13}$$

or

$$C(w) = \int_0^\infty 2w\, \eta_0(\xi)\, J_0(2w\sqrt{\xi})\, d\xi, \tag{2.14}$$

after changing dummy variable x of the integral with ξ.

Finally, the free surface elevation can be given as

$$\eta(x,t) = \int_0^\infty \left[\int_0^\infty 2w\, \eta_0(\xi)\, J_0(2w\sqrt{\xi})\, d\xi \right] J_0(2w\sqrt{x})\, e^{-iwt}\, dw. \tag{2.15}$$

2.2.2 Series Solution Formulation

The governing equation (2.4) can also be solved in a finite domain, $0 \leq x \leq L$ and $0 \leq t$, as an initial-boundary value problem with eigenvalue expansion, i.e. as a classical separation of variables problem, similar to Aydın and Kânoğlu (2017), instead of the integral transform technique presented in the previous section. In this case, initial-boundary value problem has a solution as an eigenvalue expansion under the most general condition, that is an initial wave height distribution, $\eta(x, t = 0) = \eta_0(x)$, with a corresponding initial velocity profile, $u(x, t = 0) = u_0(x) \neq 0$.

Separating the variables, $\eta(x,t) = S(x)T(t)$, equation (2.4) becomes

$$\frac{S_x}{S} + x\frac{S_{xx}}{S} = \frac{T_{tt}}{T} = -\lambda^2, \tag{2.16}$$

where λ is a real separation constant. Then, the separated equations become

$$x\, S_{xx} + S_x + \lambda^2 S = 0, \tag{2.17a}$$

$$T_{tt} + \lambda^2 T = 0. \tag{2.17b}$$

The solutions of equations (2.17a) and (2.17b) are

$$S(x) = C_1\, J_0(2\lambda\sqrt{x}) + C_2\, Y_0(2\lambda\sqrt{x}), \tag{2.18a}$$

$$T(t) = C_3 \cos(\lambda t) + C_4 \sin(\lambda t), \tag{2.18b}$$

respectively, where J_0 and Y_0 are the first and the second kind Bessel functions, and C_1, C_2, C_3, and C_4 are arbitrary constants. Hence, the solution of the governing equation (2.4) takes the following form

$$\begin{aligned}\eta(x,t) &= S(x)T(t) \\ &= \Big[C_1\, J_0(2\lambda\sqrt{x}) + C_2\, Y_0(2\lambda\sqrt{x})\Big]\Big[C_3\cos(\lambda t) + C_4\sin(\lambda t)\Big].\end{aligned} \tag{2.19}$$

The arbitrary constants could be determined considering the following initial and boundary conditions. First, finite solution at the shoreline as in the previous solution, $\eta(x=0,t) = finite$, requires C_2 to be zero since $Y_0(2\lambda\sqrt{x}) \to -\infty$ when $x \to 0$. Hence, the solution (2.19) reduces to

$$\eta(x,t) = C_1\, J_0(2\lambda\sqrt{x})\Big[C_3\cos(\lambda t) + C_4\sin(\lambda t)\Big]. \tag{2.20}$$

Next, Dirichlet (first-type) boundary condition at the seaward boundary ($x = L$) is assumed in order to allow for a simpler formulation for eigenvalue expansion, i.e. $\eta(x=L,t) = 0$, which results

$$J_0(2\lambda\sqrt{L}) = 0. \tag{2.21}$$

Therefore, eigenvalues are

$$\lambda_n = \overline{z}_n = \frac{z_n}{2\sqrt{L}}. \tag{2.22}$$

Note that $\overline{z}_n$'s are the eigenvalues of the problem where z_n's are the zeros[1] of the Bessel function of the first kind of order zero, J_0. Hence, the series solution for $\eta(x,t)$ becomes

$$\eta(x,t) = \sum_{n=1}^{\infty} J_0(2\overline{z}_n\sqrt{x})\,\Big[A_n\,\cos(\overline{z}_n t) + B_n\,\sin(\overline{z}_n t)\Big], \tag{2.23}$$

after substituting (2.22) into the equation (2.20). Also, substitution of equation (2.23) into equation (2.3a), $u_t = -\eta_x$, leads

$$u(x,t) = \sum_{n=1}^{\infty} \frac{J_1(2\overline{z}_n\sqrt{x})}{\sqrt{x}}\,\Big[A_n\,\sin(\overline{z}_n t) - B_n\,\cos(\overline{z}_n t)\Big]. \tag{2.24}$$

The coefficients A_n and B_n are calculated imposing the following initial conditions,

[1] The first few zeros of the function $J_0(z)$ are: $z_1 = 2.405$, $z_2 = 5.520$, $z_3 = 8.654$, $z_4 = 11.792, \ldots$.

$\eta(x, t = 0) = \eta_0(x)$ and $\eta_t(x, t = 0) = u_0(x)$ and obtained as

$$\eta_0(x) = \sum_{n=1}^{\infty} A_n \, J_0(2\overline{z}_n\sqrt{x}), \tag{2.25a}$$

$$u_0(x) = \sum_{n=1}^{\infty} \overline{z}_n B_n \, J_0(2\overline{z}_n\sqrt{x}). \tag{2.25b}$$

Multiplying both sides of equations (2.25a) and (2.25b) with $J_0(2\overline{z}_m\sqrt{x})$ and integrating along the domain of solution we get

$$\int_0^L \eta_0(x) \, J_0(2\overline{z}_n\sqrt{x})dx = L \, J_1^2(z_n) \, A_n, \tag{2.26a}$$

$$\int_0^L u_0(x) \, J_0(2\overline{z}_n\sqrt{x})dx = \overline{z}_n L J_1^2(z_n) \, B_n, \tag{2.26b}$$

using orthogonality of Bessel functions defined as

$$\int_0^L J_0(2\overline{z}_n\sqrt{x}) \, J_0(2\overline{z}_m\sqrt{x})dx = L \, J_1^2(z_n) \, \delta_{nm}, \tag{2.27}$$

where δ_{nm} represents Kronecker's delta. Hence, the unknown coefficients A_n and B_n are calculated as

$$A_n = \frac{1}{L \, J_1^2(z_n)} \int_0^L \eta_0(x) J_0(2\overline{z}_n\sqrt{x})dx, \tag{2.28a}$$

$$B_n = \frac{1}{z_n \, L \, J_1^2(z_n)} \int_0^L u_0(x) J_0(2\overline{z}_n\sqrt{x})dx, \tag{2.28b}$$

where $(n \geq 1)$.

The shoreline quantities are now calculated by simply substituting $x = 0$ in equations (2.23) and (2.24). Hence, temporal variation of the shoreline free-surface height is given as

$$\eta(0, t) = \eta_s(t) = \sum_{n=1}^{\infty} \Big[A_n \, \cos(\overline{z}_n t) + B_n \, \sin(\overline{z}_n t) \Big], \tag{2.29}$$

from equation (2.23) and temporal variation of the shoreline velocity is given as

$$u(0, t) = u_s(t) = \sum_{n=1}^{\infty} \overline{z}_n \Big[A_n \, \sin(\overline{z}_n t) - B_n \, \cos(\overline{z}_n t) \Big], \tag{2.30}$$

from equation (2.24). Note that the singularity of the velocity at the shoreline can be avoided considering

$$\lim_{x \to 0} \frac{J_1(2\overline{z}_n\sqrt{x})}{\sqrt{x}} = \overline{z}_n.$$

2.3 Application to Different Initial Wave Profiles

In this section, the linear solution methodologies developed in Section 2.2 are applied to the initial wave profiles introduced in Carrier et al. (2003) and the results are compared with the nonlinear solution of Kânoğlu (2004). The wave profiles considered are Gaussian wave, solitary wave, and isosceles and generalized *N*-waves. In these applications, the seaward boundary is selected to be at $L = 50$ for the series solution so that waves reflected from the artificial seaward boundary do not affect the nearshore solution. Initial waves introduced here extend to infinity theoretically. However, L is chosen large enough to have wave height practically zero at the seaward boundary initially.

2.3.1 Gaussian Wave Type Initial Conditions

Carrier et al. (2003) define a Gaussian initial wave profile as

$$\eta_0(x) = H_1 \, \mathrm{e}^{-c_1(x-x_1)^2}, \tag{2.31}$$

where H_1 is the initial wave height, c_1 is the steepness of the profile and x_1 is the initial location of the wave maximum, respectively. Further, they define *N*-wave as a combination of two Gaussian waves

$$\eta_0(x) = H_1 \, \mathrm{e}^{-c_1(x-x_1)^2} - H_2 \, \mathrm{e}^{-c_2(x-x_2)^2}. \tag{2.32}$$

According to (2.15), the free surface elevation $\eta(x,t)$ resulting from the integral transform solution for this *N*-wave configuration can be given as

$$\eta(x,t) = \int_0^\infty 2\big(H_1 \, \mathrm{e}^{-c_1(\xi-x_1)^2} - H_2 \, \mathrm{e}^{-c_2(\xi-x_2)^2}\big) \times \left[\int_0^\infty w J_0(2w\sqrt{\xi}) J_0(2w\sqrt{x}) e^{-iwt} \, dw \right] d\xi \, . \tag{2.33}$$

For the series solution method, the free surface elevation can be calculated by using (2.23) and (2.28) as

$$\eta(x,t) = \sum_{n=1}^{\infty} J_0(2\overline{z}_n\sqrt{x}) \left[\frac{1}{L \, J_1^2(z_n)} \int_0^L \big(H_1 \, \mathrm{e}^{-c_1(\xi-x_1)^2} - H_2 \, \mathrm{e}^{-c_2(\xi-x_2)^2}\big) \times J_0(2\overline{z}_n\sqrt{\xi}) d\xi \right] \cos(\overline{z}_n t). \tag{2.34}$$

The solutions (2.33) and (2.34) are given for zero initial velocity condition. The initial wave profiles used in the presented solution methodologies are shown in Figure 2.2 and their parameters are listed in Table 2.1.

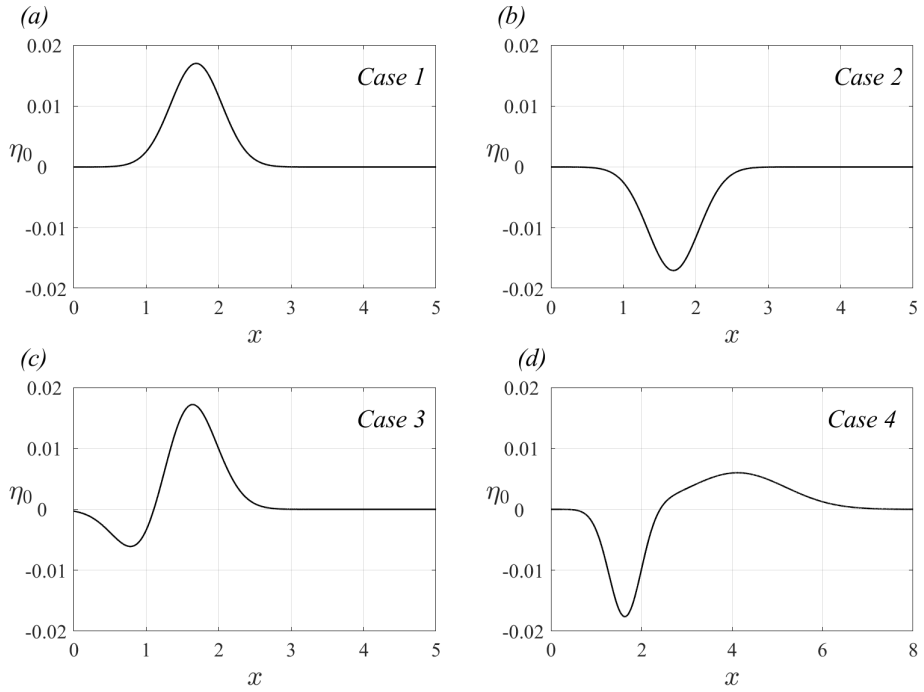

Figure 2.2: The initial wave profiles given by Carrier et al. (2003); (a) positive Gaussian wave, (b) negative Gaussian wave, (c-d) Gaussian *N*-waves. The wave parameters used to define these initial waves are listed in Table 2.1.

Table 2.1: Parameters for the initial waveforms given in Figure 2.2 (Carrier et al., 2003).

	H_1	c_1	x_1	H_2	c_2	x_2
Case 1	0.017	4.0	1.69	-	-	-
Case 2	-0.017	4.0	1.69	-	-	-
Case 3	0.020	3.5	1.5625	0.010	3.5	1.0
Case 4	0.006	0.4444	4.1209	0.018	4.0	1.6384

2.3.1.1 Results for Zero Initial Velocity Case

The spatial and temporal variations of water surface elevations are calculated using both the integral transform and the series solution methods, i.e. equations (2.33) and (2.34) for the initial waveforms given in Figure 2.2 and the results are presented in Figures 2.3 and 2.4.

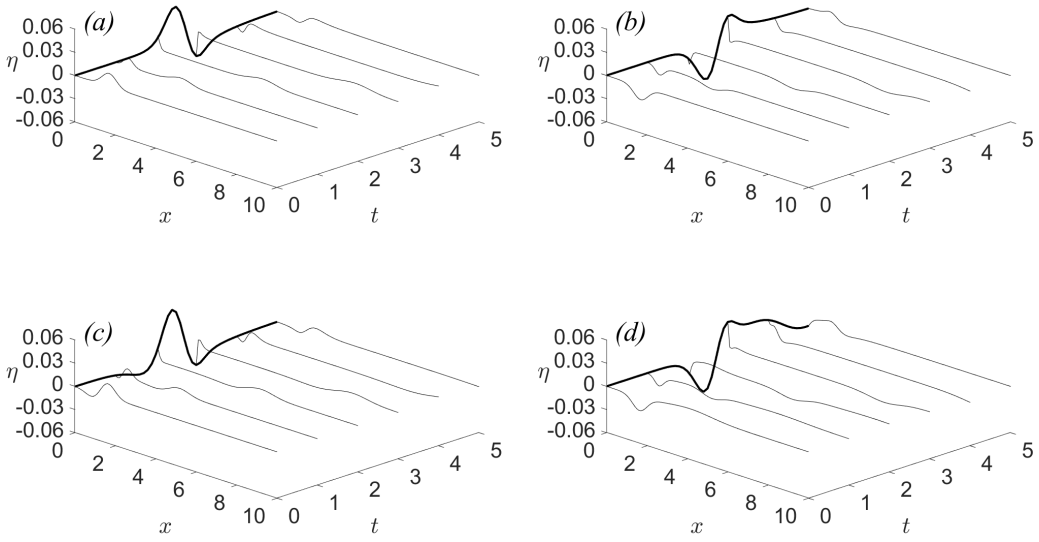

Figure 2.3: Spatial and temporal variations of (thin lines) the water surface elevation including (thick lines) shoreline motion obtained from the integral solution for (a) positive Gaussian wave, Case 1, (b) negative Gaussian wave, Case 2, (c-d) Gaussian *N*-waves, Case 3 and Case 4, defined by Carrier et al. (2003).

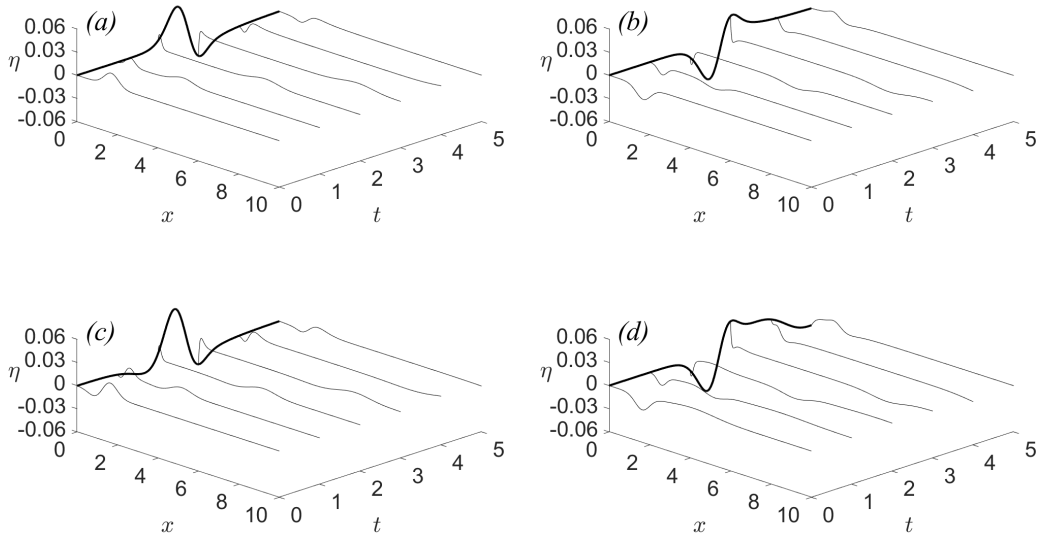

Figure 2.4: Spatial and temporal variations of (thin lines) the water surface elevations including (thick lines) shoreline motions obtained from the series solution for (a) positive Gaussian wave, Case 1, (b) negative Gaussian wave, Case 2, (c-d) Gaussian *N*-waves, Case 3 and Case 4, defined by Carrier et al. (2003).

In Figures 2.5 and 2.6, spatial variations of the free surface elevation η for Case 1 are compared with linear solution methodologies for zero initial velocity condition. The shoreline wave heights η_s and the shoreline velocities u_s are compared for the results of the solutions introduced here, linear integral and series solutions, and the results of nonlinear solution (Kânoğlu, 2004) in Figure 2.7 in the case of zero initial velocity condition. Also, the maximum and minimum values of shoreline wave heights and the shoreline velocities are listed and compared in Table 2.2.

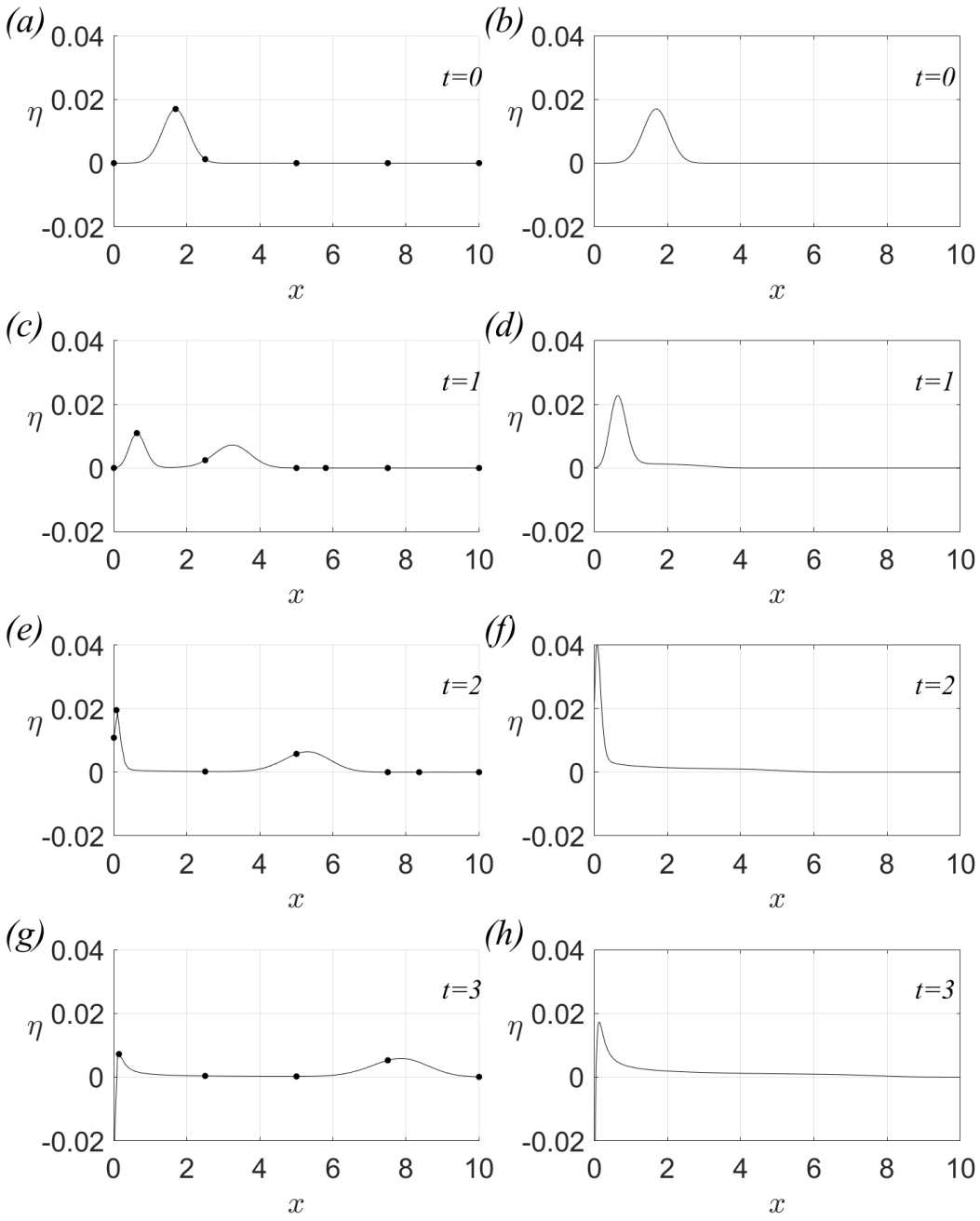

Figure 2.5: Spatial variations of wave heights η for the positive Gaussian wave (Case 1), given in Figure 2.2a, (left insets) results from integral and series solution methodologies with zero initial velocity and (right insets) results from series solution with nonzero initial velocity. Solid lines represent the series solution results, while dots represent the integral solution results.

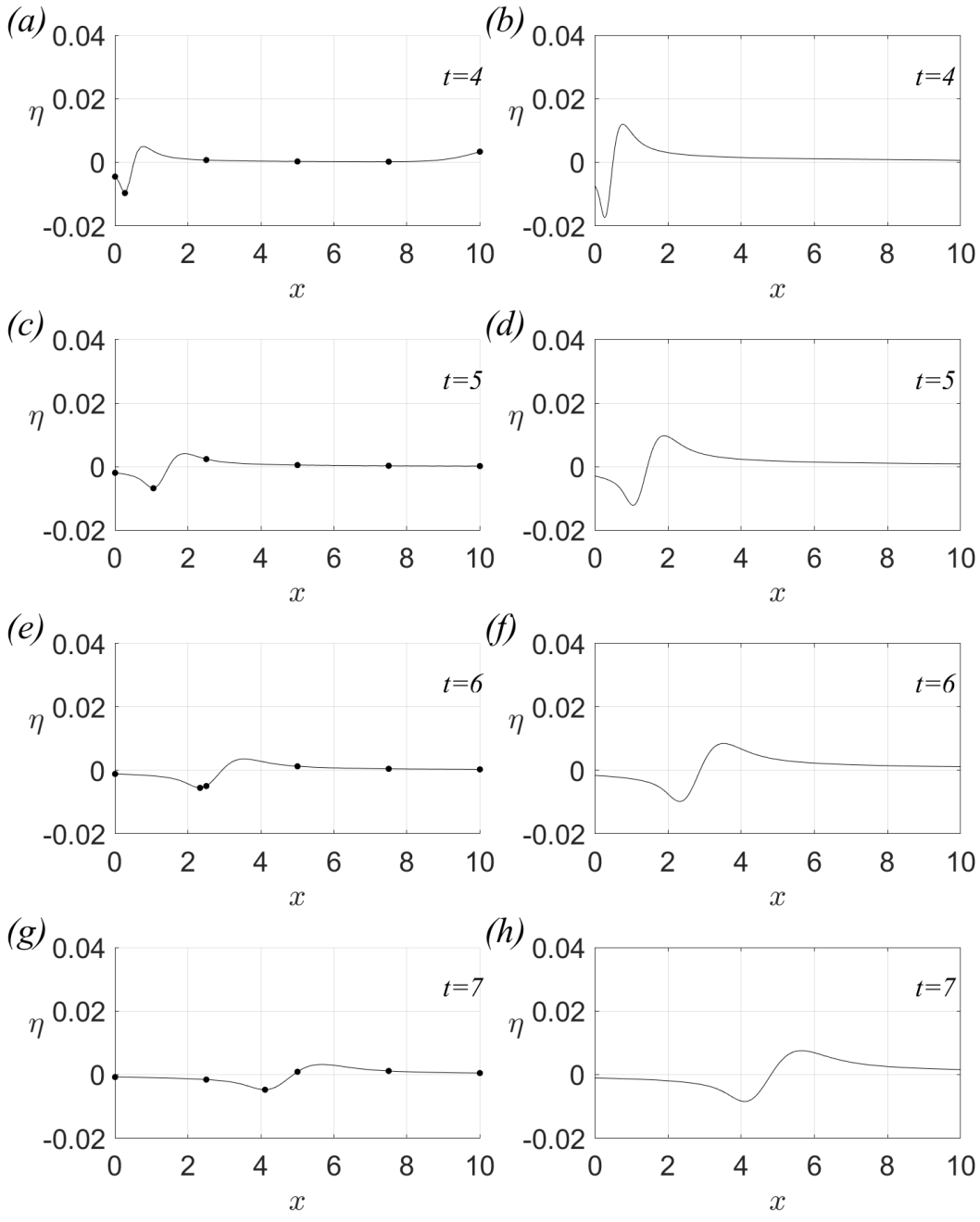

Figure 2.6: Continued from Figure 2.5

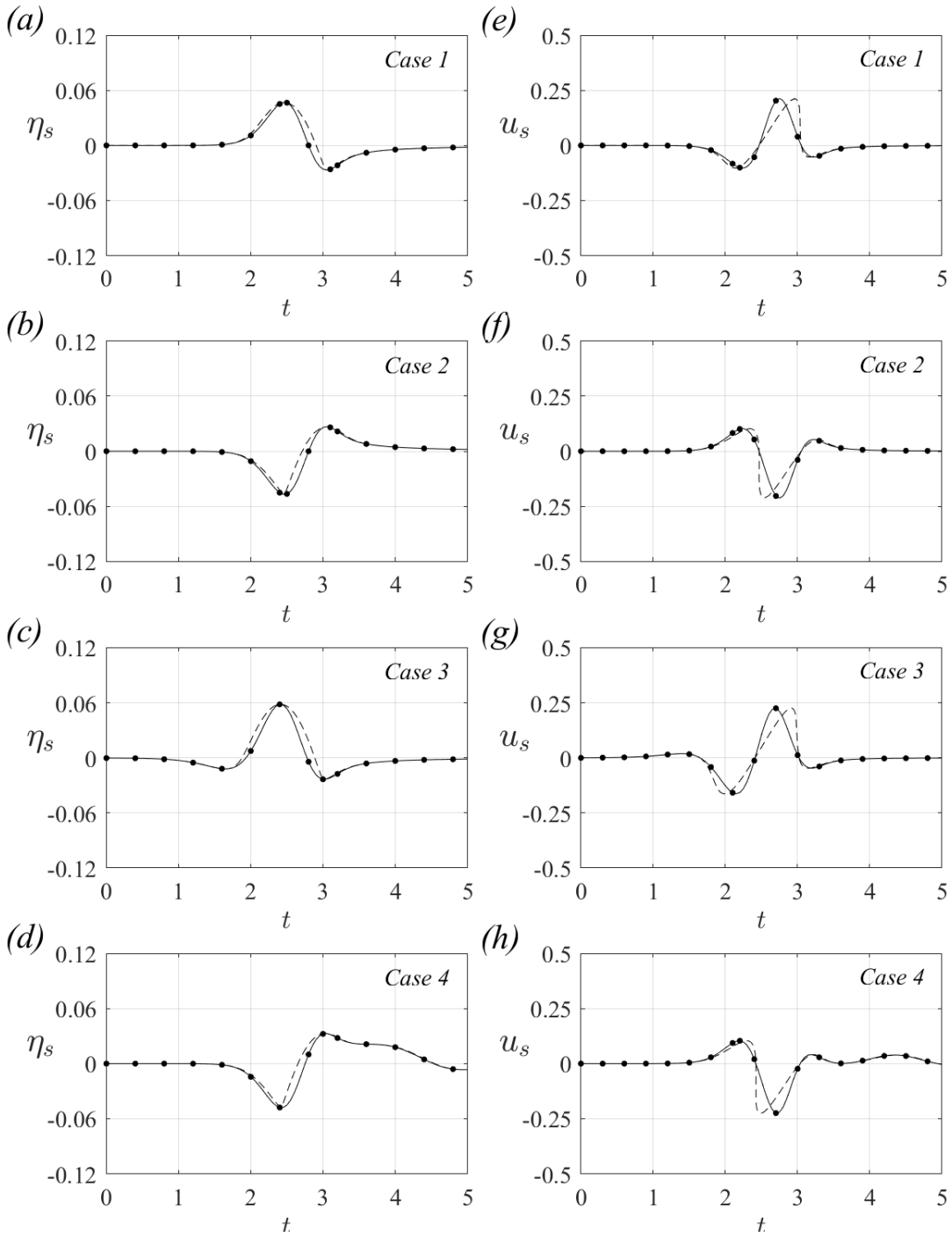

Figure 2.7: Temporal variations of (left insets) the shoreline wave heights η_s and (right insets) the shoreline velocities u_s for the initial wave profiles given in Figure 2.2 without initial velocity. Solid and dashed lines represent the integral transform solution and nonlinear solution of Kânoğlu (2004), respectively, while dots represent the series solution results. The maximum runup and minimum rundown values are tabulated in Table 2.2.

Table 2.2: Comparison of extreme values between the present integral formulation and series solution techniques, and Kânoğlu (2004)'s solution.

		Case 1	*Case 2*	*Case 3*	*Case 4*
Maximum runup	Integral transform	0.0465	0.0260	0.0583	0.0324
	Series solution	0.0469	0.0268	0.0583	0.0327
	Kânoğlu (2004)	0.0470	0.0268	0.0583	0.0328
Maximum rundown	Integral transform	-0.0260	-0.0465	-0.0233	-0.0478
	Series solution	-0.0268	-0.0465	-0.0233	-0.0478
	Kânoğlu (2004)	-0.0268	-0.0470	-0.0235	-0.0484
Maximum shoreward velocity	Integral Solution	-0.1027	-0.2131	-0.1634	-0.2253
	Series Solution	-0.1026	-0.2132	-0.1634	-0.2252
	Kânoğlu (2004)	-0.1026	-0.2131	-0.1632	-0.2253
Maximum seaward velocity	Integral Solution	0.2130	0.1028	0.2256	0.1036
	Series Solution	0.2131	0.1026	0.2256	0.1036
	Kânoğlu (2004)	0.2130	0.1030	0.2260	0.1040

2.3.1.2 Results for Nonzero Initial Velocity Case

In this section, results of the series solution of the linear shallow water-wave equation is presented for the cases introduced in Section 2.3 having nonzero initial velocity profiles. Nonzero initial velocity assumption is implemented as in Carrier et al. (2003), i.e. linear approximation for the initial velocity,

$$u_0(x) = -\frac{\eta_0(x)}{\sqrt{h(x)}} = -\frac{\eta_0(x)}{\sqrt{x}}. \tag{2.35}$$

Minus sign is introduced here to allow initial wave to propagate toward to the shoreline.

The effect of having initial velocity is also investigated using linear series solution methodology. In Figures 2.5 and 2.6, spatial variations of wave height are given for Case 1 of Carrier et al. (2003) and compare with the case zero initial velocity. In Figure 2.8, the shoreline wave heights η_s and the shoreline velocities u_s are compared for the cases with nonzero and zero initial velocity conditions. In addition, linear series solution results are compared with the results from the nonlinear solution of Aydın and Kânoğlu (2017). The maximum and minimum values of the shoreline wave heights η_s and the shoreline velocities u_s are listed in Table 2.3.

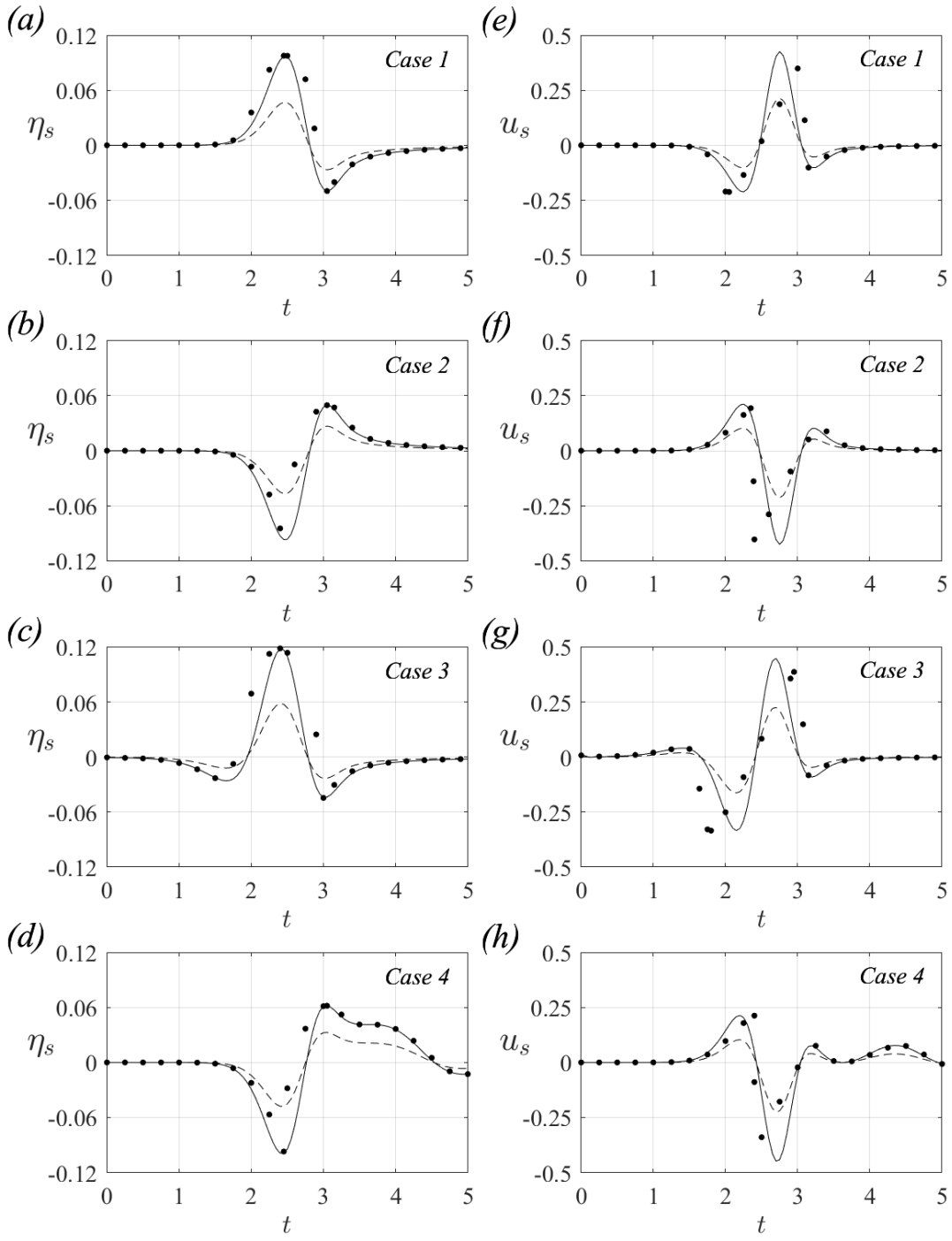

Figure 2.8: Temporal variations of (left insets) the shoreline wave heights, η_s, and (right insets) the shoreline velocities, u_s, for the Gaussian and *N*-wave initial wave profiles given in Figure 2.2. Solid and dashed lines represent the nonzero and zero initial velocity conditions for the present series solution, respectively, while dots represent the results of nonlinear series solution of Aydın and Kânoğlu (2017) with nonzero initial velocity. The maximum runup and minimum rundown values are tabulated in Table 2.3.

Table 2.3: The maximum runup and minimum rundown values for the cases with and without initial velocity. Also the results of the nonlinear solution of Aydın and Kânoğlu (2017) is given with initial velocity.

	Without Initial Velocity ($u_0 = 0$)				With Initial Velocity ($u_0 \neq 0$)				Aydın and Kânoğlu (2017) ($u_0 \neq 0$)			
	η_{max}	η_{min}	u_{max}	u_{min}	η_{max}	η_{min}	u_{max}	u_{min}	η_{max}	η_{min}	u_{max}	u_{min}
Case 1	0.0469	-0.0268	0.2131	-0.1026	0.0969	-0.0498	0.4257	-0.2117	0.0978	-0.0501	0.3763	-0.2132
Case 2	0.0268	-0.0469	0.1026	-0.2131	0.0498	-0.0969	0.2117	-0.4257	0.0497	-0.1095	0.2070	-0.4185
Case 3	0.0583	-0.0233	0.2250	-0.1634	0.1178	-0.0438	0.4480	-0.3343	0.1186	-0.0446	0.4067	-0.3358
Case 4	0.0327	-0.0478	0.1035	-0.2245	0.0620	-0.0991	0.2138	-0.4482	0.0619	-0.1020	0.2126	-0.3547

2.3.2 Solitary Wave Type Initial Condition

A solitary wave is defined as

$$\eta_0(x) = H \text{ sech}^2\gamma_s\,(x - x_1), \tag{2.36}$$

where $\gamma_s = \sqrt{3H/4}$. In this definition, H is the initial height and x_1 is the initial location of the maximum of wave. Once a solitary wave is introduced over a sloping beach without initial velocity, according to (2.15), free surface elevation $\eta(x,t)$ resulting from the integral transform solution is given as

$$\eta(x,t) = \int_0^\infty 2\big[H \text{ sech}^2\gamma_s\,(\xi - x_1)\big]\times \left[\int_0^\infty wJ_0(2w\sqrt{\xi})J_0(2w\sqrt{x})e^{-iwt}\,dw\right] d\xi\,. \tag{2.37}$$

For the series solution, free surface elevation is calculated by using (2.23) and (2.28) as

$$\eta(x,t) = \sum_{n=1}^{\infty} J_0(2\overline{z}_n\sqrt{x})\left[\frac{1}{L\,J_1^2(z_n)}\int_0^L H \text{ sech}^2\gamma_s\,(\xi - x_1)\times J_0(2\overline{z}_n\sqrt{\xi})d\xi\right]\cos(\overline{z}_n t), \tag{2.38}$$

again for solitary wave initial form without initial velocity.

Kânoğlu (2004) calculated the shoreline height and velocity of the solitary wave initial condition with the parameters $H = 0.03$ and $x_1 = 20$ (Figure 2.9a) without initial velocity. The spatial and temporal variations of the water surface elevations are calculated with the integral transform and series solution techniques using equations (2.37) and (2.38), and presented in Figure 2.10. The shoreline wave height η_s and the shoreline velocity u_s are compared for the integral solution and series solution in Figure 2.9b-c. The maximum and minimum values of shoreline wave heights and the shoreline velocities are also given in Table 2.4 for both solution methodologies. Several initial wave heights are considered in Figure 2.9d. Maximum runup of solitary wave follows $R \sim H^{5/4}$ as in Synolakis (1987)'s result ($R = 2.831\sqrt{\cot\,\beta}\;H^{5/4}$). Even though Synolakis (1987) derived the maximum runup formula for the canonical problem with a different normalization, as similar observation ($R \sim H^{5/4}$) made here as in Kânoğlu (2004) with nonlinear solution.

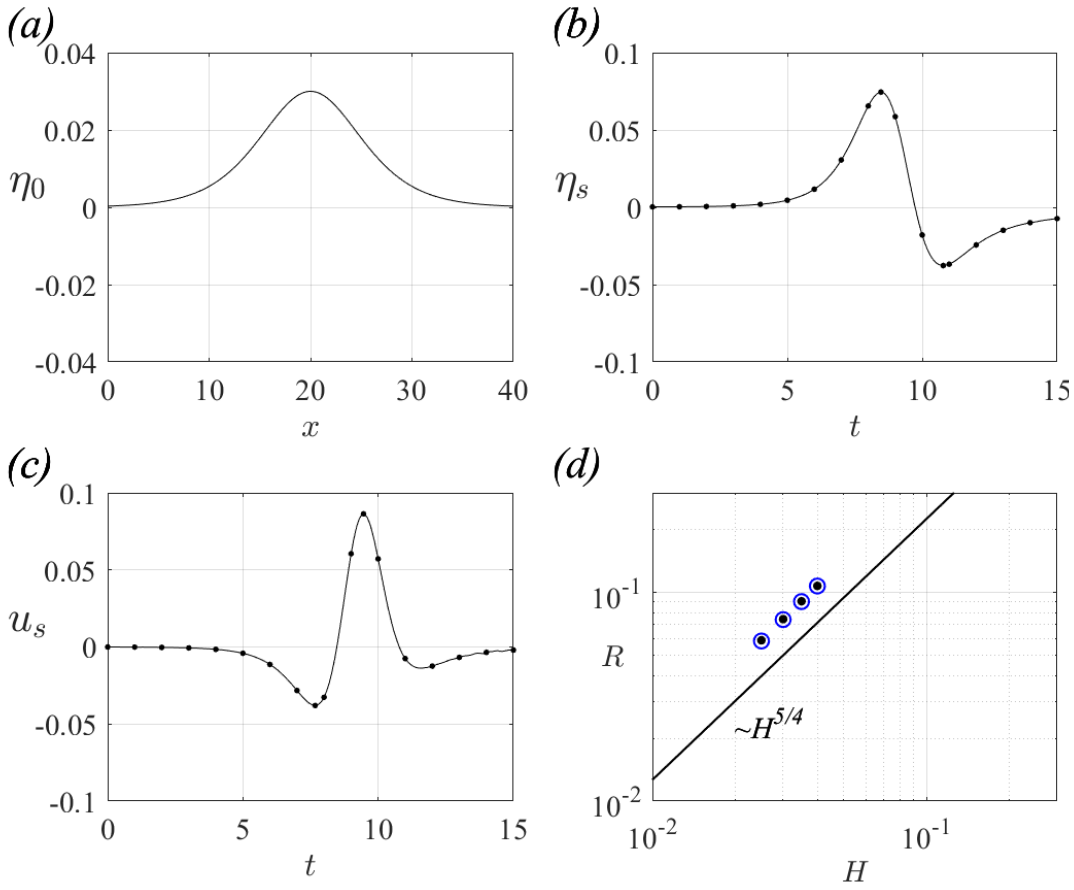

Figure 2.9: The runup-rundown characteristics of solitary wave initial waveform, (a) initial wave profile with $H = 0.03$, $x_1 = 20$, (b) temporal variation of the shoreline wave height η_s and (c) shoreline velocity u_s for (solid line) integral and (dots) series solutions, (d) maximum runup of solitary waves with $H = 0.04$, 0.035, 0.03 and 0.025 at $x_1 = 20$; (dots) the linear series solution for presented here and (circles) the nonlinear solution of Kânoğlu (2004).

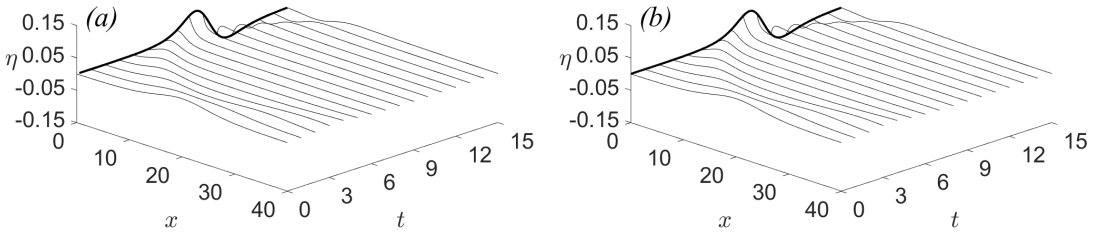

Figure 2.10: Spatial and temporal variations of (thin lines) the water surface elevations including (thick lines) shoreline motions calculated with (a) integral and (b) series solutions for the solitary wave with $H = 0.03$ and $x_1 = 20$.

Table 2.4: Comparison of the maximum runup and minimum rundown for solitary wave with the integral transform and series solution techniques. Refer to the caption of Figure 2.9.

	η_{max}	η_{min}	u_{max}	u_{min}
Integral Solution	0.074473	-0.037683	0.086136	-0.037918
Series Solution	0.074511	-0.037692	0.086374	-0.037692

2.3.3 Isosceles *N*-Wave Type Initial Condition

Tadepalli and Synolakis (1994) introduced a waveform, which has the same wave height at depression and elevation sides and called as isosceles *N*-wave. An isosceles *N*-wave is defined as

$$\eta_0(x) = \frac{3\sqrt{3}}{2}\, H\, \text{sech}^2\gamma_s\,(x - x_1)\, \text{tanh}\gamma_s\,(x - x_1), \tag{2.39}$$

where $\gamma_s = (3/2)\sqrt{H\sqrt{3/4}}$. In this definition, H is the initial wave height and x_1 locates the initial wave.

According to (2.15), free surface elevation $\eta(x,t)$ for an isosceles *N*-wave is

$$\eta(x,t) = \int_0^\infty 2\Big[\frac{3\sqrt{3}}{2}\, H\, \text{sech}^2\gamma_s\,(\xi - x_1)\, \text{tanh}\gamma_s\,(\xi - x_1)\Big] \times \Big[\int_0^\infty w J_0(2w\sqrt{\xi}) J_0(2w\sqrt{x}) e^{-iwt}\, dw\Big]\, d\xi, \tag{2.40}$$

for zero initial wave velocity. For the series solution, the free surface elevation is calculated by using (2.23) and (2.28) as

$$\eta(x,t) = \sum_{n=1} J_0(2\overline{z}_n\sqrt{x}) \left[\frac{1}{L\, J_1^2(z_n)} \int_0^L \frac{3\sqrt{3}}{2}\, H\, \text{sech}^2\gamma_s\,(\xi - x_1)\times \right.$$
$$\left. \tanh\,\gamma_s\,(\xi - x_1) J_0(2\overline{z}_n\sqrt{\xi}) d\xi \right] \cos(\overline{z}_n t). \tag{2.41}$$

again for zero initial velocity case.

Kânoğlu (2004) presented nonliner solution for two examples of the isosceles *N*-waves, leading-depression isosceles *N*-wave, η_d, and leading-elevation isosceles *N*-wave, $\eta_e = -\eta_d$, with parameters $H = 0.03$ and $x_1 = 15$ (Figure 2.11a and e, respectively). The spatial and temporal variations of water surface elevations of the same initial wave are calculated with the integral and series solution techniques, and presented in Figures 2.12 and 2.13 using equations (2.40) and (2.41). The shoreline wave height η_s and the shoreline velocity u_s of the leading-depression and -elevation isosceles *N*-waves are compared for the integral and series methodologies in Figure 2.11 with zero initial velocity condition, $u_0 = 0$. The maximum and minimum values of shoreline wave heights and the shoreline velocities are also summarized in Table 2.5. Several cases are considered in Figure 2.11 for leading-depression and -elevation isosceles *N*-wave forms as in Kânoğlu (2004). Maximum runup of isosceles *N*-wave follows $R \sim H^{5/4}$ as in Tadepalli and Synolakis (1994)'s result ($R = 3.86\sqrt{\cot\,\beta}\, H^{5/4}$). Even though Tadepalli and Synolakis (1994) derived the maximum runup formula for the canonical problem with a different normalization, as similar observation ($R \sim H^{5/4}$) made here as in nonlinear solution of Kânoğlu (2004).

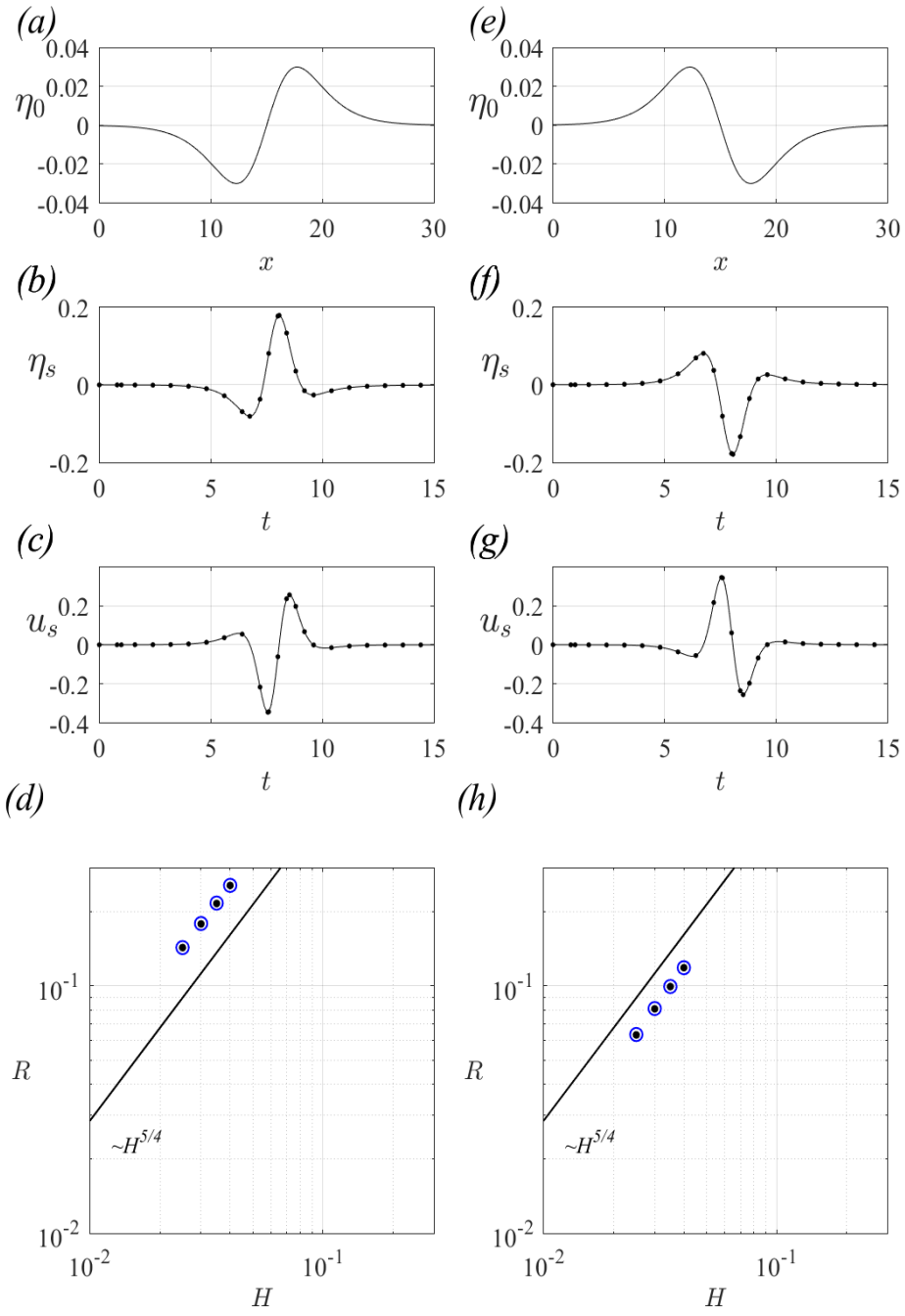

Figure 2.11: The runup-rundown characteristics of isosceles (left insets) leading-depression $\eta_d(x,0)$ and (right insets) leading-elevation *N*-waves ($\eta_e(x,0) = -\eta_d(x,0)$) with $H = 0.03$, $x_1 = 15$. (a, e) The initial wave profiles, (b, f) temporal variations of the shoreline wave heights η_s and (c, g) shoreline velocities u_s for (solid line) integral and (dots) series solution. (d, h) The maximum runup of the leading-depression and leading-elevation isosceles *N*-waves with $H = 0.04$, 0.035, 0.03 and 0.025 at $x_1 = 15$ are shown for (dots) linear series solution presented here and (circles) the nonlinear solution of Kânoğlu (2004).

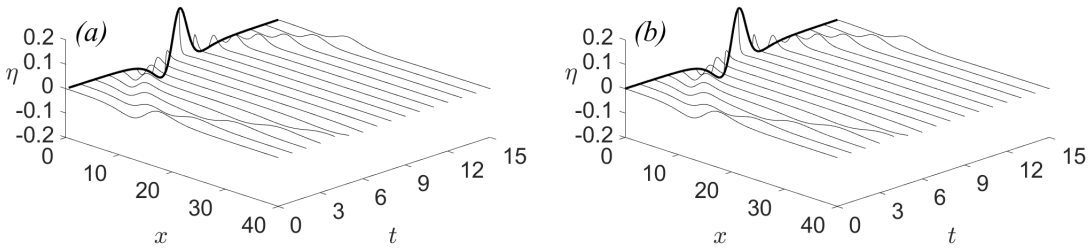

Figure 2.12: Spatial and temporal variations of (thin lines) the water surface elevation including (thick lines) shoreline motions for (a) integral solution and (b) series solution for the leading-depression isosceles *N*-wave with $H = 0.03$ and $x_1 = 15$.

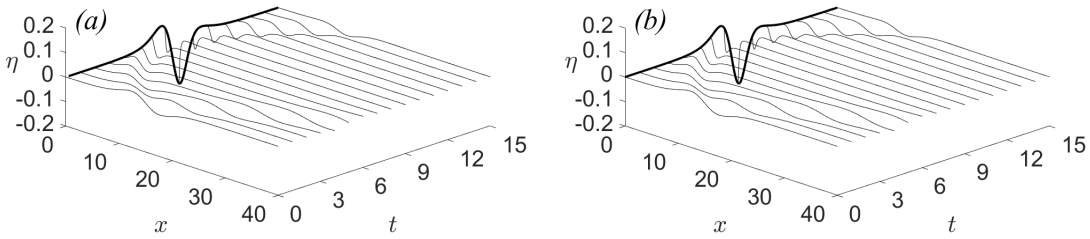

Figure 2.13: Spatial and temporal variations of (thin lines) the water surface elevation including (thick lines) shoreline motions for (a) integral solution and (b) series solution for the leading-elevation isosceles *N*-wave with $H = 0.03$ and $x_1 = 15$.

Table 2.5: Comparison of the maximum runup and minimum rundown values for the given leading-depression and leading-elevation isosceles *N*-waves for the integral and series solution methodologies. Refer to the caption of Figure 2.11.

	Leading-Depression Isosceles N-wave				*Leading-Elevation Isosceles N-wave*			
	η_{max}	η_{min}	u_{max}	u_{min}	η_{max}	η_{min}	u_{max}	u_{min}
Integral Solution	0.177929	-0.080769	0.255126	-0.341837	0.080769	-0.177929	0.341837	-0.255126
Series Solution	0.178732	-0.081037	0.255624	-0.345142	0.081037	-0.178732	0.345142	-0.255624

2.3.4 Generalized *N*-Wave Type Initial Condition

Tadepalli and Synolakis (1996) also introduced a waveform, which produces positive and negative disturbances with different heights, as an alternative model to isosceles *N*-waves which are called as generalized *N*-waves. A generalized *N*-wave is defined as

$$\eta_0(x) = \varepsilon\, H\, (x - x_2)\, \text{sech}^2\gamma_s\, (x - x_1), \tag{2.42}$$

where $\gamma_s = \sqrt{3\, H/4}$. In this definition, ε is a scaling parameter to provide a wave with initial maximum height H and x_1 is the initial location of the wave.

According to (2.15), free surface elevation $\eta(x,t)$ for the generalized *N*-wave is

$$\eta(x,t) = \int_0^\infty 2\varepsilon\, H\, (\xi - x_2)\, \text{sech}^2\gamma_s\, (\xi - x_1) \times \left[\int_0^\infty w J_0(2w\sqrt{\xi}) J_0(2w\sqrt{x}) e^{-iwt}\, dw \right] d\xi. \tag{2.43}$$

for zero initial wave velocity. For the series solution, the free surface elevation can be calculated by using (2.23) and (2.28) as

$$\eta(x,t) = \sum_{n=1} J_0(2\overline{z}_n\sqrt{x}) \left[\frac{1}{L\, J_1^2(z_n)} \int_0^L \left(\varepsilon\, H\, (\xi - x_2)\, \text{sech}^2\gamma_s\, (\xi - x_1)\right) \times J_0(2\overline{z}_n\sqrt{\xi}) d\xi \right] \cos(\overline{z}_n t). \tag{2.44}$$

again for zero initial velocity.

Kânoğlu (2004) presented nonlinear solution for two examples of the generalized *N*-wave as initial condition, leading-depression generalized *N*-wave with parameters $H = 0.06$, $\varepsilon = 0.2$, $x_1 = 18$ and $x_2 = 17$, and leading-elevation generalized *N*-wave with parameters $H = 0.06$, $\varepsilon = 0.2$, $x_1 = 24.2$ and $x_2 = 25.2$ (Figure 2.14a and e). The shoreline wave heights, η_s, and the shoreline velocities, u_s, of the leading-depression generalized *N*-wave are compared on integral and series solution in Figure 2.14 with the zero initial velocity condition, $u_0 = 0$. The maximum and minimum values of shoreline wave heights and the shoreline velocities are given in Table 2.6. The spatial and temporal variations of the water surface elevation of the same initial wave are calculated with integral and series solution techniques, and presented in Figures 2.15 and 2.16.

Several cases are considered in Figure 2.14d and h for leading-depression and -elevation generalized *N*-wave forms as in Kânoğlu (2004). Maximum runup of generalized *N*-waves follow $R \sim H^{3/4}$ as in Tadepalli and Synolakis (1994)'s result ($R = 2.831\varepsilon\sqrt{\cot\ \beta}\, H^{5/4}\,[|X_1 - X_2 - 0.366/\gamma| + 0.618/\gamma]$). Even though Tadepalli and Synolakis (1994) derived the maximum runup formula for the canonical problem with a different normalization, as similar observation ($R \sim H^{3/4}$) made here as in Kânoğlu (2004) with nonlinear solution.

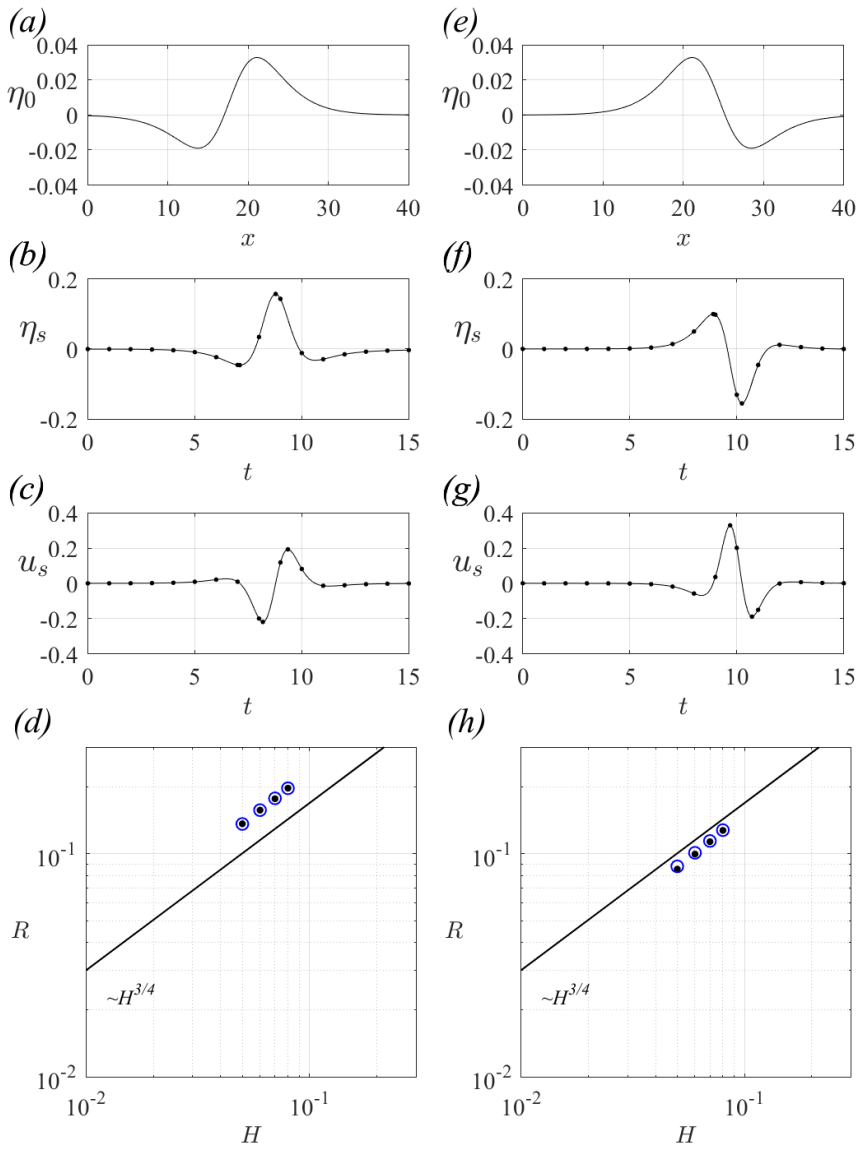

Figure 2.14: The runup and rundown characteristics of (left insets) the leading-depression ($H = 0.06$, $\varepsilon = 0.2$, $x_1 = 18$ and $x_2 = 17$) and (right insets) leading-elevation ($H = 0.06$, $\varepsilon = 0.2$, $x_1 = 24.20$ and $x_2 = 25.20$) generalized *N*-wave profiles. (a, e) The initial wave profiles, (b, f) temporal variations of the shoreline wave heights η_s and (c, g) shoreline velocities u_s for (solid line) integral and (dots) series solution, (d) the maximum runup of the leading-depression generalized *N*-waves with $H = 0.08, 0.07, 0.06$ and 0.05 for $\varepsilon = 0.2$, $x_1 = 18$ and $x_2 = 17$ are shown for (dots) linear series solution presented here and (circles) the nonlinear solution of Kânoğlu (2004) and (h) the maximum runup of the leading-elevation generalized *N*-waves with $\varepsilon = 0, 2$, $x_1 - x_2 = -1$ and $x_1 = 23.24, 23.66, 24.20$ and 24.88 for $H = 0.08, 0.07, 0.06$ and 0.05 are shown for (dots) results of the linear series solution presented here and (circles) the nonlinear solution of Kânoğlu (2004).

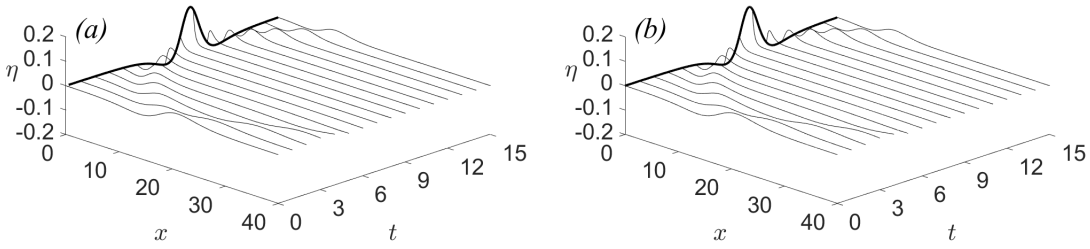

Figure 2.15: Spatial and temporal variations of (thin lines) the water surface elevation including (thick lines) shoreline motions for the leading-depression generalized *N*-wave with $H = 0.06$, $\varepsilon = 0N.2$, $x_1 = 18$ and $x_2 = 17$.

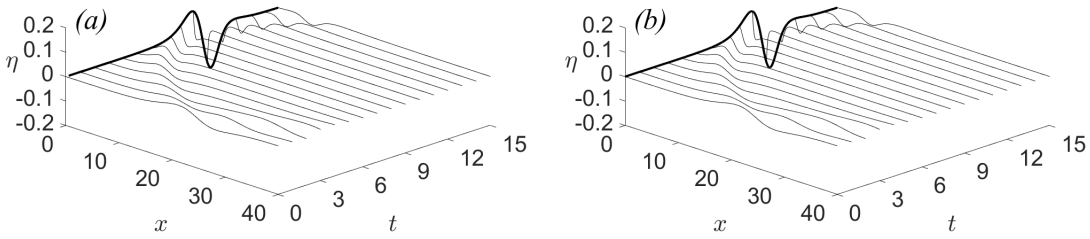

Figure 2.16: Spatial and temporal variations of (thin lines) the water surface elevation including (thick lines) shoreline motions for the leading-elevation generalized *N*-wave with $H = 0.06$, $\varepsilon = 0.2$, $x_1 = 24.2$ and $x_2 = 25.2$.

Table 2.6: Comparison of the maximum runup and minimum rundown for the given leading-depression and -elevation generalized *N*-wave with the integral and series solution techniques. Refer to the caption of Figure 2.14.

	Leading-Depression Generalized N-wave				*Leading-Elevation Generalized N-wave*			
	η_{max}	η_{min}	u_{max}	u_{min}	η_{max}	η_{min}	u_{max}	u_{min}
Integral Solution	0.156911	-0.046090	0.191664	-0.219136	0.099743	-0.154796	0.329033	-0.189200
Series Solution	0.157079	-0.046090	0.192898	-0.219279	0.099744	-0.155590	0.329319	-0.189299

2.4 Conclusion

The linear shallow water-wave equations are solved using integral formulation methodology similar to Kânoğlu (2004) and eigenvalue expansion similar to Aydın and Kânoğlu (2017) over a sloping beach as an initial-boundary value problem. Comparisons of the results of the linear solutions with nonlinear solution show the runup invariance between the linear and nonlinear solutions, i.e. both theories produce different propagation yet they produce same maximum runup.

In addition, the linear solution does not include hodograph transforms; hence, it is much more simpler than the nonlinear solutions. Also, the series solution uses eigenfunction expansion rather than integral transforms, which makes the present series solution method more efficient in terms of computation time and effort.

CHAPTER 3

RUNUP OF NEAR-SHORE LONG WAVES ON A SLOPING BEACH

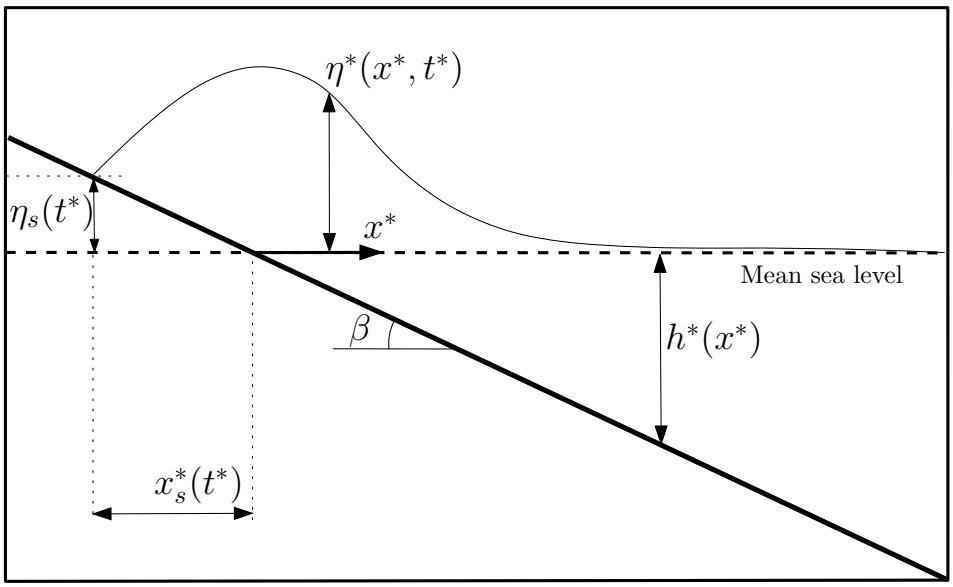

Figure 3.1: The definition sketch (not to scale).

In dimensional form, the nonlinear shallow water-wave equations are given as

$$u^*_{t^*} + u^*\, u^*_{x^*} + g^* \eta^*_{x^*} = 0, \tag{3.1a}$$

$$\left[u^*(h^* + \eta^*)\right]_{x^*} + \eta^*_{t^*} = 0, \tag{3.1b}$$

where $u^* = u^*(x^*, t^*)$ and $\eta^* = \eta^*(x^*, t^*)$ represent the depth-averaged velocity and the free-surface elevation, respectively. The variable depth $h^*(x^*)$ can be defined as $h^*(x) = x^* \tan\beta$ where β is the beach angle from the horizontal. After defining the dimensionless variables as

$$u = \frac{u^*}{\sqrt{l_0^*\, g^*\, \tan\beta}}, \quad \eta, h = \frac{\eta^*, h^*}{l_0^*\, \tan\beta}, \quad x = \frac{x^*}{l_0^*}, \quad t = \frac{t^*}{\sqrt{l_0^*/g^*\, \tan\beta}}, \tag{3.2}$$

where l_0^* is a characteristic length scale and g^* is the gravitational acceleration. The dimensionless form of the nonlinear shallow water-wave equations can be written, in view of equations (3.2), as

$$u_t + u\,u_x + \eta_x = 0, \tag{3.3a}$$

$$[u(h+\eta)]_x + \eta_t = 0. \tag{3.3b}$$

Carrier and Greenspan (1958) introduced the following transformation, hence called Carrier–Greenspan transformation

$$x = \frac{1}{16}\sigma^2 - \frac{1}{4}\phi_\lambda + \frac{1}{2}u^2, \tag{3.4a}$$

$$t = u - \frac{1}{2}\lambda, \tag{3.4b}$$

$$u = \frac{\phi_\sigma}{\sigma}, \tag{3.4c}$$

$$\eta = \frac{1}{4}\phi_\lambda - \frac{1}{2}u^2, \tag{3.4d}$$

and they were able to reduce equations (3.3) into the following differential equation

$$\sigma\phi_{\lambda\lambda} - (\sigma\,\phi_\sigma)_\sigma = 0. \tag{3.5}$$

Given initial wave profile in (σ, λ)–space, i.e. $\eta(\sigma, \lambda = 0)$, which corresponds $t = 0$ in the absence of initial velocity, i.e. $u = 0$, the solution of (3.5) is

$$\phi(\sigma,\lambda) = -\int_0^\infty \omega^{-1} J_0(\omega\sigma)\sin(\omega\lambda)d\omega \int_0^\infty \xi^2 J_1(\omega\xi)\Phi(\xi)d\xi, \tag{3.6}$$

and, from (3.4),

$$u(\sigma,\lambda) = \int_0^\infty \sigma^{-1} J_1(\omega\sigma)\sin(\omega\lambda)d\omega \int_0^\infty \xi^2 J_1(\omega\xi)\Phi(\xi)d\xi, \tag{3.7}$$

where $\Phi(\sigma) = u_\lambda(\sigma, 0) = 4\eta_\sigma(\sigma, 0)/\sigma$ (Carrier and Greenspan, 1958). Hence, the evolution of water surface elevation is now given by

$$\begin{aligned}\eta(\sigma,\lambda) = \frac{1}{4}\phi_\lambda - \frac{1}{2}u^2 = -\frac{1}{4}\left\{\int_0^\infty \xi^2\Phi(\xi)\left[\int_0^\infty J_0(\omega\sigma)\,J_1(\omega\xi)\cos(\omega\lambda)d\omega\right]d\xi\right\} \\ -\frac{1}{2}\left\{\int_0^\infty \xi^2\Phi(\xi)\left[\int_0^\infty \frac{J_1(\omega\sigma)}{\sigma}J_1(\omega\xi)\sin(\omega\lambda)d\omega\right]d\xi\right\}^2.\end{aligned} \tag{3.8}$$

Major difficulty in Carrier and Greenspan (1958)'s solution was how to transform the initial condition given in (x,t)–space into the (σ,λ)–space. Kânoğlu (2004) proposed the linearized form of the hodograph transformation $x \cong \frac{1}{16}\sigma^2$, which can be used when defining the initial waveform in (σ,λ)–space as $\eta(\frac{1}{16}\sigma^2,0)$ after defining the initial waveform in (x,t)–space as $\eta(x,0)$. Hence, the evolution of initial waveform can be calculated with a straightforward integration after considering $\Phi(\sigma) = 4\eta_\sigma(\frac{1}{16}\sigma^2,0)/\sigma$. Further, equation (3.8) can be written for the shoreline runup-rundown motion as

$$\begin{aligned}\eta_s(\lambda) = \frac{1}{4}\phi_\lambda - \frac{1}{2}u_s^2 = -\frac{1}{4}\left\{\int_0^\infty \xi^2\Phi(\xi)\left[\int_0^\infty J_1(\omega\xi)\cos(\omega\lambda)d\omega\right]d\xi\right\} \\ -\frac{1}{2}\left\{\int_0^\infty \xi^2\Phi(\xi)\left[\int_0^\infty \frac{1}{2}\omega J_1(\omega\xi)\sin(\omega\lambda)d\omega\right]d\xi\right\}^2.\end{aligned} \tag{3.9}$$

since $\sigma = 0$ at the shoreline. Moreover, Kânoğlu (2004) simplified the solution for the shoreline velocitiy $u_s(\lambda) = u(0,\lambda)$ as

$$u_s = -\lambda\Phi(0) - \frac{1}{2}\int_0^\lambda \frac{2\lambda^2-\xi^2}{\sqrt{\lambda^2-\xi^2}}\frac{d\phi(\xi)}{d\xi}d\xi. \tag{3.10}$$

and the shoreline wave height $\eta_s(\lambda) = \eta(0,\lambda)$ as

$$\begin{aligned}\eta_s(\lambda) = \frac{1}{4}\phi_\lambda - \frac{1}{2}u_s^2 = -\frac{1}{4}\left[\int_0^\infty \xi\Phi(\xi)d\xi - \lambda^2\Phi(0) - \int_0^\lambda \lambda\sqrt{\lambda^2-\xi^2}\frac{d\Phi(\xi)}{d\xi}d\xi\right] \\ -\frac{1}{2}\left[-\lambda\Phi(0) - \frac{1}{2}\int_0^\lambda \frac{2\lambda^2-\xi^2}{\sqrt{\lambda^2-\xi^2}}\frac{d\Phi(\xi)}{d\xi}d\xi\right]^2.\end{aligned} \tag{3.11}$$

Further, Tinti and Tonini (2005) obtained an analytical solution for propagation of tsunamis resulting from near-shore earthquakes. They use Carrier and Greenspan (1958)'s solution as presented in (3.6) and (3.7) with $u_\lambda(\sigma,0) = \Phi(\sigma) = 4\eta_\sigma(\sigma,0)/\sigma$. Further, in the hodograph space, they assumed the following initial waveform for near-shore earthquakes

$$\begin{aligned}\eta_0(\sigma) &= \sum_{k=0}^{3} c_k(1+\sigma^2)^{-(k+3/2)} \\ &= c_0(1+\sigma^2)^{-3/2} + c_1(1+\sigma^2)^{-5/2} + c_2(1+\sigma^2)^{-7/2} + c_3(1+\sigma^2)^{-9/2}.\end{aligned} \tag{3.12}$$

After substantial algebra, Tinti and Tonini (2005) first gives analytical expression for spatial and temporal evolution of long waves. Then, they reduce expressions for shoreline velocity $u_c(0,\lambda)$ as

$$u_c(\lambda) = u(0,\lambda) = -4\left(c_0 + \frac{c_1}{3} + \frac{c_2}{5} + \frac{c_3}{7}\right)\mathrm{Im}\left\{\frac{1}{p^3}\right\} - 4\left(\frac{c_1}{3} + \frac{c_2}{5} + \frac{c_3}{7}\right)\mathrm{Im}\left\{\frac{3}{p^4}\right\} - 4\left(\frac{c_2}{5} + \frac{6c_3}{35}\right)\mathrm{Im}\left\{\frac{4}{p^5}\right\} - 4\frac{c_3}{7}\mathrm{Im}\left\{\frac{4}{p^6}\right\}, \tag{3.13}$$

and shoreline elevation $\eta_c(0,\lambda)$ as

$$\eta_c(\lambda) = \eta(0,\lambda) = \left(c_0 + \frac{c_1}{3} + \frac{c_2}{5} + \frac{c_3}{7}\right)\mathrm{Re}\left\{\frac{1}{p^2}\right\} + \left(\frac{c_1}{3} + \frac{c_2}{5} + \frac{c_3}{7}\right)\mathrm{Re}\left\{\frac{2}{p^3}\right\} + \left(\frac{c_2}{5} + \frac{c_3}{35}\right)\mathrm{Re}\left\{\frac{2}{p^4}\right\} + \frac{6c_3}{35}\mathrm{Re}\left\{\frac{8}{p^5}\right\} - \frac{{u_c}^2}{2}, \tag{3.14}$$

where $p = (1 - i\lambda)$. Hence, their solution not only involves substantial algebra but also calculation with complex numbers. However, Tinti and Tonini (2005) could have used their initial waveform (3.12) directly in Kânoğlu (2004)'s solution, which would have avoid substantion algebra involved.

3.1 New Mathematical Formulation

In this subsection, the initial waveform given by Tinti and Tonini (2005) is used with Kânoğlu (2004)'s methodology. The procedure is described below in details.

Given initial waveform in the transform space as in equation (3.12), initial condition for the solution can be written as

$$\begin{aligned}\Phi(\sigma) &= \frac{4\eta_\sigma(\sigma,0)}{\sigma} \\ &= -8(1+\sigma^2)^{-5/2}\sum_{k=0}^{3}(\frac{3}{2}+k)\,c_k\,(1+\sigma^2)^{-k} \\ &= -\frac{12c_0}{(1+\sigma^2)^{5/2}} - \frac{20c_1}{(1+\sigma^2)^{7/2}} - \frac{28c_2}{(1+\sigma^2)^{9/2}} - \frac{36c_3}{(1+\sigma^2)^{11/2}},\end{aligned} \tag{3.15}$$

which leads to

$$\frac{d\Phi(\sigma)}{d\sigma} = \frac{4\sigma[15c_0(1+\sigma^2)^3 + 35c_1(1+\sigma^2)^2 + 63c_2(1+\sigma^2) + 99c_3}{(1+\sigma^2)^{13/2}}. \tag{3.16}$$

Then, the following integrals can be calculated analytically to calculate u_s and η_s

$$\Phi(0) = -4(3c_0 + 5c_1 + 7c_2 + 9c_3), \tag{3.17a}$$

$$\begin{aligned}\int_0^\lambda \frac{2\lambda^2 - \xi^2}{\sqrt{\lambda^2 - \xi^2}} \frac{d\Phi(\xi)}{d\xi} d\xi = \frac{8\lambda^3}{105(1+\lambda^2)^6}[&105c_0(1+\lambda^2)^3(10 + 9\lambda^2 + 3\lambda^4) \\ &+ 35c_1(1+\lambda^2)^2(70 + 91\lambda^2 + 60\lambda^4 + 15\lambda^6) \\ &+ 21c_2(210 + 567\lambda^2 + 708\lambda^4 + 526\lambda^6 + 210\lambda^8 + 35\lambda^{10}) \\ &+ 3c_3(2310 + 4851\lambda^2 + 6336\lambda^4 + 4730\lambda^6 + 1890\lambda^8 + 315\lambda^{10})],\end{aligned} \tag{3.17b}$$

$$\int_0^\infty \xi\Phi(\xi) d\xi = -4(c_0 + c_1 + c_2 + c_3), \tag{3.17c}$$

and

$$\begin{aligned}\int_0^\lambda \lambda\sqrt{\lambda^2 - \xi^2} \frac{d\Phi(\xi)}{d\xi} d\xi = \frac{4\lambda^4}{105(1+\lambda^2)^5}\Big[&105c_0(1+\lambda^2)^3(5 + 3\lambda^2) \\ &+ 35c_1(1+\lambda^2)^2(35 + 42\lambda^2 + 15\lambda^4) \\ &+ 21c_2(1+\lambda^2)(105 + 189\lambda^2 + 135\lambda^4 + 35\lambda^6) \\ &+ 3c_3(1155 + 2772\lambda^2 + 5\lambda^4(594 + 308\lambda^2 + 63\lambda^4)\Big].\end{aligned} \tag{3.17d}$$

Hence, the shoreline velocity can be given through equation (3.10) as

$$\begin{aligned}u_s(\sigma = 0, \lambda) = -\frac{4\lambda}{105(1+\lambda^2)^6}[&105c_0(1+\lambda^2)^3(-3 + \lambda^2) \\ &+ 35c_1(1+\lambda^2)^2(-15 + 10\lambda^2 + \lambda^4) \\ &+ 21c_2(-35 + 42\lambda^4 + 8\lambda^6 + \lambda^8) \\ &+ 3c_3(-315 + 420\lambda^2 + 126\lambda^4 + 36\lambda^6 + 5\lambda^8)],\end{aligned} \tag{3.18}$$

using equations (3.17a) and (3.17b). Then, the shoreline wave height $\eta_s(\sigma = 0, \lambda)$ becomes

$$\begin{aligned}\eta_s(\lambda) = c_0 + c_1 + c_2 + c_3 - (3c_0 + 5c_1 + 7c_2 + 9c_3)\lambda^2 - \frac{8\lambda^2}{11025(1+\lambda^2)^{12}}\times \\ \big[105c_0(-3+\lambda^2)(1+\lambda^2)^3 + 35c_1(1+\lambda^2)^2(-15+10\lambda^2+\lambda^4) \\ + 21c_2(-35+42\lambda^4+8\lambda^6+\lambda^8) + 3c_3(-315+420\lambda^2+126\lambda^4+36\lambda^6+5\lambda^8)\big]^2 \\ + \frac{\lambda^4}{105(1+\lambda^2)^5}\big[105c_0(1+\lambda^2)^3(5+3\lambda^2) + 35c_1(1+\lambda^2)^2(35+42\lambda^2+15\lambda^4) \\ + 3(735c_2+1155c_3+42(49c_2+66c_3)\lambda^2+54(42c_2+55c_3)\lambda^4 \\ + 70(17c_2+22c_3)\lambda^6+35(7c_2+9c_3)\lambda^8)\big],\end{aligned} \tag{3.19}$$

using (3.17c), (3.17d) and (3.18) in (3.11). Equations (3.4) then provides $x_s = -\eta_s$ and $t_s = u_s - \frac{1}{2}\lambda$.

3.2 Results for Different Initial Waveforms

Tinti and Tonini (2005) chose four different near-shore earthquake configurations to confirm the form of equation (3.12) as an initial wave profile. They derived the initial vertical coseismic movements for coastal earthquakes by using Okada's dislocation model (Okada; 1985, 1992). Then, they curvefit (3.12) to Okada (1985)'s deformation. Initial profiles used by Tinti and Tonini (2005) are shown in Figure 3.2 and the coefficients c_k's determined by using curve fitting are given in Table 3.1.

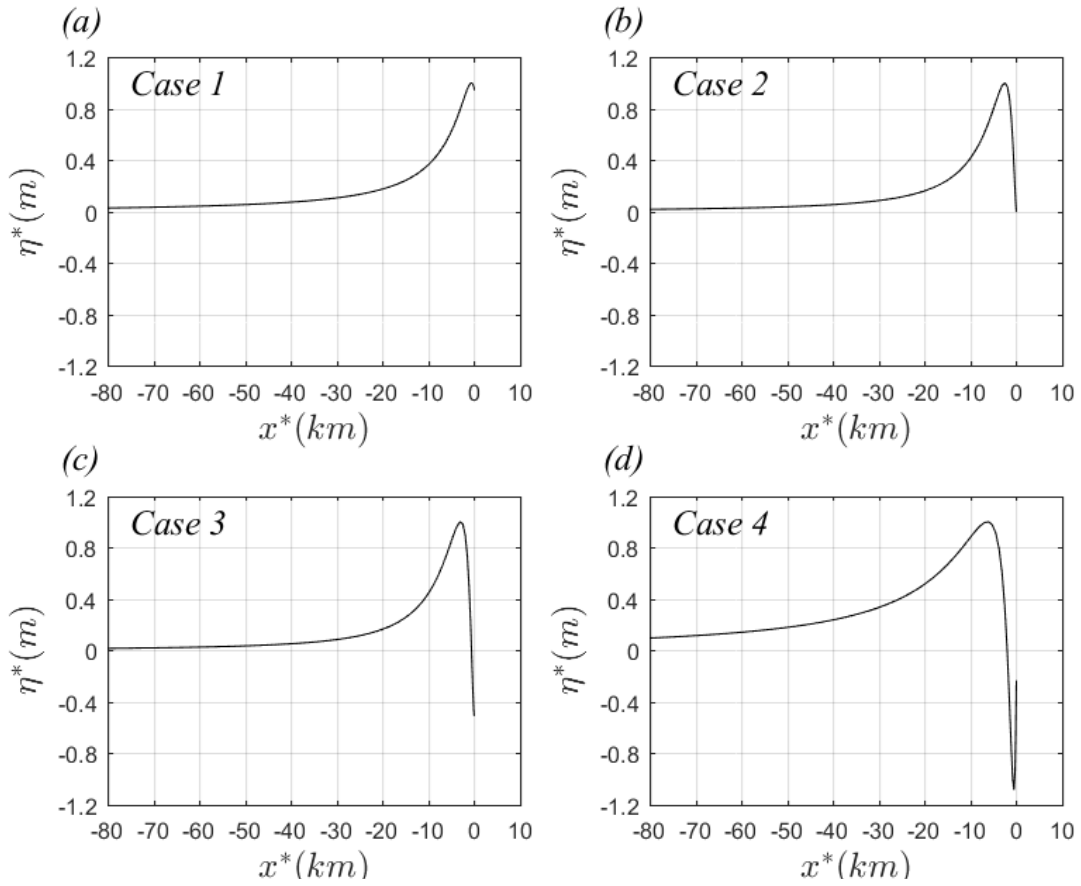

Figure 3.2: The initial wave profiles used by Tinti and Tonini (2005). The coefficients in (3.12) are listed in Table 3.1 for each parameter. The dimensional quantities are calculated using the characteristic length of $l_0^* = 50\ km$ and beach slope of $\tan\beta = 1/25$, leading to the characteristic depth of $l_0^* \tan\beta = 2000\ m$. Case 1 is a vertical fault located inland; Case 2 is the same vertical fault which is located under the shoreline. Case 3 is also the same vertical fault is placed slightly offshore. The last configuration, Case 4, consists of the combination of a dominant inverse two-segment and an ancillary surface normal faults which are placed under the seabed. Refer to Tinti and Tonini (2005) for corresponding earthquake source parameters.

Table 3.1: The coefficients in equation (3.12) for the cases presented in Figure 3.2 (Tinti & Tonini, 2005).

	c_0	c_1	c_2	c_3
Case 1	2.046E-03	-2.127E-03	5.526E-04	1.750E-07
Case 2	9.979E-04	6.634E-03	-1.580E-02	8.170E-03
Case 3	7.399E-04	9.559E-03	-2.230E-02	1.175E-02
Case 4	7.106E-03	-1.438E-02	2.797E-04	6.881E-03

In Figures 3.3-3.6, the solutions through equations (3.18) and (3.19) are compared with Tinti and Tonini (2005)'s solution with exact agreement as expected. Yet, solution presented here is much simpler than Tinti and Tonini (2005)'s methodology, since it does not involve computations with complex numbers.

3.3 Conclusion

Tinti and Tonini (2005)'s initial waveform is implemented in Kânoğlu (2004)'s shoreline solution. Results reveal that the solution presented here is much simpler and does not involve complex algebra. Hence, it allows calculation of maximum runup in a much simpler way.

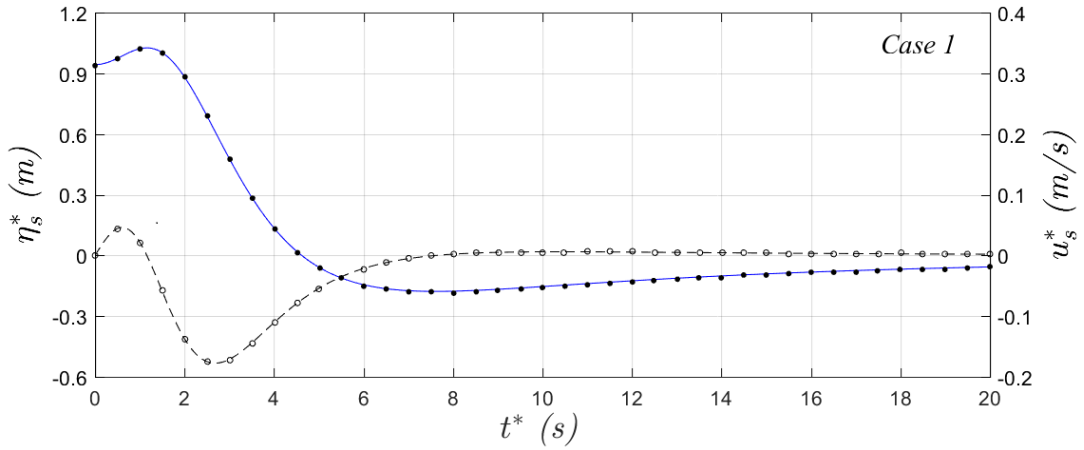

Figure 3.3: Time evolution of the shoreline wave height η_s^* and the shoreline velocity u_s^* for Tinti and Tonini (2005)'s Case 1. Solid and dashed lines represent the shoreline wave height and the shoreline velocity for the solution presented here, respectively, while dots represent the results of Tinti and Tonini (2005). The dimensional quantities are calculated using the characteristic length of $l_0^* = 50\ km$ and beach slope of $\tan\beta = 1/25$, leading to the characteristic depth of $l_0^* \tan\beta = 2000\ m$.

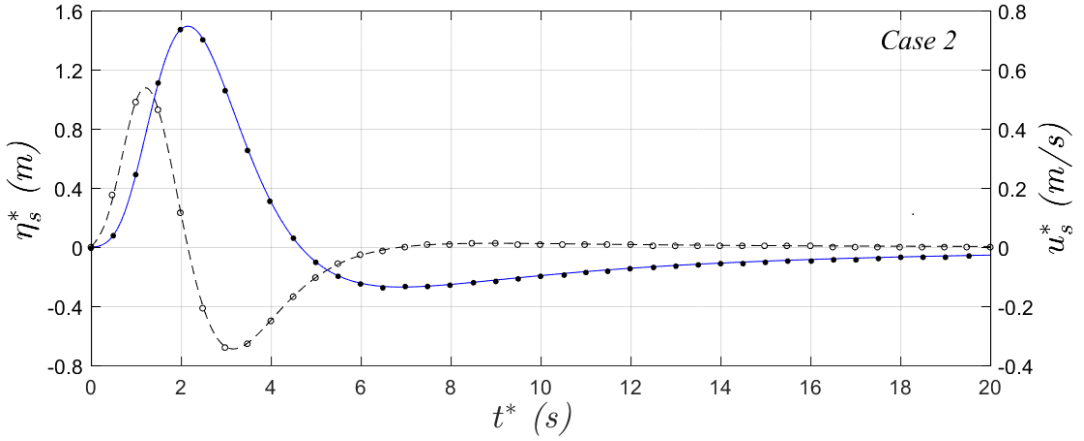

Figure 3.4: Time evolution of the shoreline wave height η_s^* and the shoreline velocity u_s^* for Tinti and Tonini (2005)'s Case 2. Solid and dashed lines represent the shoreline wave height and the shoreline velocity for the solution presented here, respectively, while dots represent the results of Tinti and Tonini (2005). The dimensional quantities are calculated using the characteristic length of $l_0^* = 50\ km$ and beach slope of $\tan\beta = 1/25$, leading to the characteristic depth of $l_0^* \tan\beta = 2000\ m$.

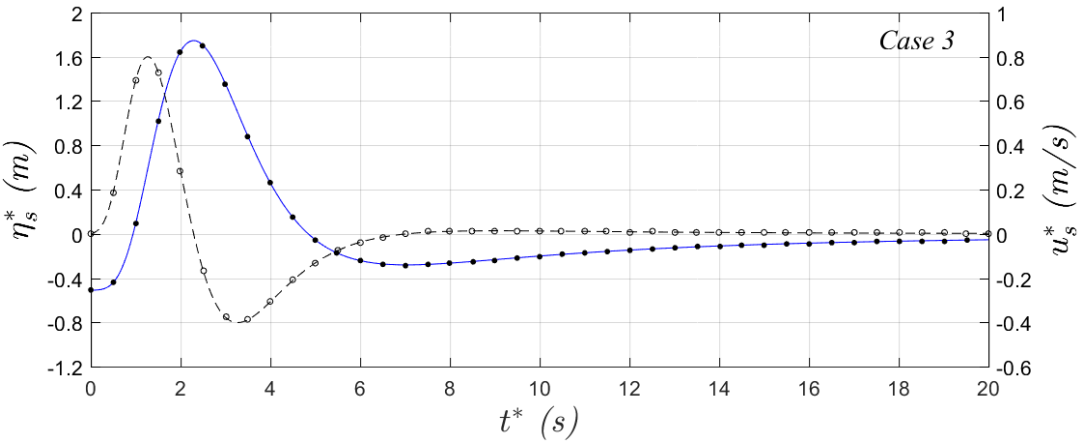

Figure 3.5: Time evolution of the shoreline wave height η_s^* and the shoreline velocity u_s^* for Tinti and Tonini (2005)'s Case 3. Solid and dashed lines represent the shoreline wave height and the shoreline velocity for the solution presented here, respectively, while dots represent the results of Tinti and Tonini (2005). The dimensional quantities are calculated using the characteristic length of $l_0^* = 50\ km$ and beach slope of $\tan\beta = 1/25$, leading to the characteristic depth of $l_0^* \tan\beta = 2000\ m$.

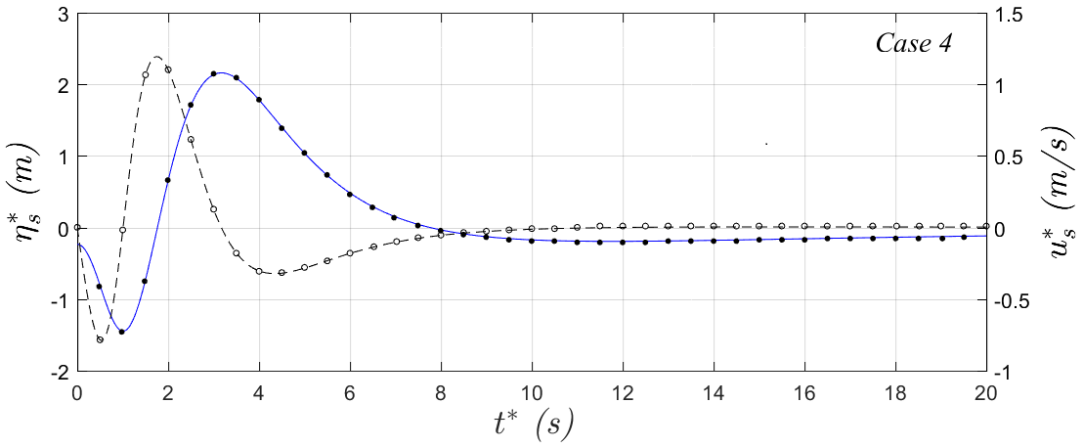

Figure 3.6: Time evolution of the shoreline wave heights η_s^* and the shoreline velocities u_s^* for Tinti and Tonini (2005)'s Case 4. Solid and dashed lines represent the shoreline wave height and the shoreline velocity for the solution presented here, respectively, while dots represent the results of Tinti and Tonini (2005). The dimensional quantities are calculated using the characteristic length of $l_0^* = 50km$ and beach slope of $\tan\beta = 1/25$, leading to the characteristic depth of $l_0^* \tan\beta = 2000\ m$.

CHAPTER 4

CONCLUSION

In this study, first, analytical solutions for the 1+1 dimensional linear shallow water-wave equations over a sloping beach are presented. Two different approach is used to solve the linear shallow water-wave equations. First, a methodology is developed using integral transform and, then, series solution method is developed using eigenvalue expansion. Then, results of solution methodologies developed here are compared with the existing solution of the nonlinear shallow water-wave equations for different initial waveforms as in Kânoğlu (2004). Results confirmed existing runup invariance between linear and nonlinear solution of the shallow water-wave equations, i.e. even though evolutions are different for these solutions they produce the same maximum runup.

Then, nonlinear solution of Kânoğlu (2004) for temporal variation of shoreline motion was used with Tinti and Tonini (2005)'s initial wave profiles. Kânoğlu (2004)'s solution is based on Carrier and Greenspan (1958) transformation which requires linearization of the transformation to define initial condition as suggested by Kânoğlu (2004). However, Tinti and Tonini (2005) presented initial waveform in the transform space for near-shore events, fitting earthquake source deformation to a specific profile. Here, their initial profile in the transform space is directly implemented to Kânoğlu (2004)'s shoreline formulation. This result much simpler formulation for the shoreline motion than Tinti and Tonini (2005)'s, which involves complex algebra, yet, results show exact comparision.

REFERENCES

Aydın, B. (2011). Analytical solutions of shallow-water wave equations. *PhD thesis, Middle East Technical University*.

Aydın, B., & Kânoğlu, U. (2017). New analytical solution for nonlinear shallow water-wave equations. *Pure and Applied Geophysics*, *174*(8), 3209–3218. doi: 10.1007/s00024-017-1508-z

Bernard, E., & Robinson, A. (2009). Geologic effects and records of tsunamis. *The sea*, *15*, 53–91.

Bilek, S. L., Satake, K., & Sieh, K. (2007). Introduction to the special issue on the 2004 Sumatra-Andaman earthquake and the Indian Ocean Tsunami. *Bulletin of the Seismological Society of America*, *97*(1 A SUPPL.), 1–5. doi: 10.1785/0120050633

Carrier, G., & Greenspan, H. (1958). Water waves of finite amplitude on a sloping beach. *Journal of Fluid Mechanics*, *4*(1), 97–109.

Carrier, G. F., Wu, T. T., & Yeh, H. (2003). Tsunami run-up and draw-down on a plane beach. *Journal of Fluid Mechanics*, *475*(475), 79–99. doi: 10.1017/S0022112002002653

Hall, J. V., & Watts, J. W. (1953). Laboratory investigation of the vertical rise of solitary waves on impermeable slopes. *US Army, Corps of Engrs, Beach Erosion Board, Tech. Memo*, *33*(13).

International Tsunami Information Center. (2018). *Global and Regional Hazard Maps.* (`http://itic.ioc-unesco.org/images/stories/awareness_and_education/map_posters/2017_tsu_poster_20180313_a2_low_res.pdf`, Last accessed on 2019-06-03)

Kânoğlu, U., & Synolakis, C. (2015). Tsunami dynamics, forecasting, and mitigation. In *Coastal and marine hazards, risks, and disasters* (pp. 15–57). Elsevier.

Kânoğlu, U., Tanioka, Y., Okal, E. A., Baptista, M. A., & Rabinovich, A. B. (2019). Introduction to "twenty five years of modern tsunami science following the

1992 nicaragua and flores island tsunamis, volume i". *Pure and Applied Geophysics*, *176*(7), 2757–2769.

Kânoğlu, U. (2004). Nonlinear evolution and runup-rundown of long waves over a sloping beach. *Journal of Fluid Mechanics*, *513*, 363–372. doi: 10.1017/S002211200400970X

Kânoğlu, U., & Synolakis, C. (2006). Initial value problem solution of nonlinear shallow water-wave equations. *Physical Review Letters*, *97*(14), 1–4. doi: 10.1103/PhysRevLett.97.148501

Kânoğlu, U., Titov, V., Bernard, E., & Synolakis, C. (2015). Tsunamis: Bridging science, engineering and society. *Philosophical Transactions of the Royal Society A: Mathematical, Physical and Engineering Sciences*, *373*(2053), 1–24. doi: 10.1098/rsta.2014.0369

Keller, J., & Keller, H. (1964). Water wave run-up on a beach. *Office of Naval Research Department of the Navy*, 40. Retrieved from `http://oai.dtic.mil/oai/oai?verb=getRecord{&}metadataPrefix=html{&}identifier=AD0608864`

NOAA. (2018). *National Geo-physical Data Center (NGDC) / World Data Service (WDS): Global Historical Tsunami Database.* (`https://www.ngdc.noaa.gov/hazard/tsu_db.shtml`, Last accessed on 2019-05-09)

Okada, Y. (1985). Surface deformation due to shear and tensile faults in a half-space. *Bulletin of the seismological society of America*, *75*(4), 1135–1154.

Okada, Y. (1992). Internal deformation due to shear and tensile faults in a half-space. *Bulletin of the seismological society of America*, *82*(2), 1018–1040.

Rabinovich, A. B., & Thomson, R. E. (2007). The 26 december 2004 sumatra tsunami: Analysis of tide gauge data from the world ocean part 1. indian ocean and south africa. In *Tsunami and its hazards in the indian and pacific oceans* (pp. 261–308). Springer.

Synolakis, C. E. (1987). The runup of solitary waves. *Journal of Fluid Mechanics*, *185*(December 1987), 523–545. doi: 10.1017/S002211208700329X

Synolakis, C. E., & Kong, L. (2006). Runup measurements of the december 2004 indian ocean tsunami. *Earthquake Spectra*, *22*(S3), 67–91.

Tadepalli, S., & Synolakis, C. E. (1994). The run-up of N-waves on sloping beaches. *Proceedings of the Royal Society of London. Series A: Mathematical and Phys-*

ical Sciences, *445*(1923), 99–112.

Tinti, S., & Tonini, R. (2005). Analytical evolution of tsunamis induced by near-shore earthquakes on a constant-slope ocean. *Journal of Fluid Mechanics*, *(535)*, 33–64. doi: 10.1017/S0022112005004532